A novel lattice model to predict chloride diffusion coefficient of unsaturated cementitious materials based on multi-typed pore structure characteristics

Tong, Liang-yu; Xiong, Qing Xiang; Zhang, Zhidong; Chen, Xiangsheng; Ye, Guang; Liu, Qing feng

DOI
10.1016/j.cemconres.2023.107351

Publication date
2023

Document Version
Final published version

Published in
Cement and Concrete Research

Citation (APA)
Tong, L., Xiong, Q. X., Zhang, Z., Chen, X., Ye, G., & Liu, Q. F. (2023). A novel lattice model to predict chloride diffusion coefficient of unsaturated cementitious materials based on multi-typed pore structure characteristics. *Cement and Concrete Research*, *176*, Article 107351. https://doi.org/10.1016/j.cemconres.2023.107351

Cement and Concrete Research 176 (2024) 107351

Contents lists available at ScienceDirect

Cement and Concrete Research

journal homepage: www.elsevier.com/locate/cemconres

A novel lattice model to predict chloride diffusion coefficient of unsaturated cementitious materials based on multi-typed pore structure characteristics

Liang-yu Tong [a], Qing Xiang Xiong [a], Zhidong Zhang [b], Xiangsheng Chen [c], Guang Ye [d], Qing-feng Liu [a,e,*]

[a] State Key Laboratory of Ocean Engineering, School of Naval Architecture, Ocean & Civil Engineering, Shanghai Jiao Tong University, Shanghai, China
[b] Department of Civil, Environment and Geomatic Engineering, Institute for Building Materials, ETH Zürich CH-8093, Switzerland
[c] College of Civil and Transportation Engineering, Shenzhen University, Shenzhen, China
[d] Microlab, Section of Materials and Environment, Faculty of Civil Engineering and Geosciences, Delft University of Technology, 2628 CN Delft, the Netherlands
[e] Shanghai Key Laboratory for Digital Maintenance of Buildings and Infrastructure, Shanghai, China

ARTICLE INFO

Keywords:
Cementitious materials
Lattice model
Drying-wetting process
Pore structure
Chloride diffusion

ABSTRACT

This paper develops a novel lattice diffusive model to quantitatively study the chloride diffusion coefficient in unsaturated cementitious materials, in which the pore voxels are redistributed to make a better representation of a real microstructure of hardened cement paste. Considering the hierarchical microstructure and different drying-wetting cycles, water distributions in multiscale pore structures are modelled and the structure characteristics of water-filled pores, including water connectivity, water tortuosity and effective porosity, are computationally extracted based on that. A lattice diffusion network is established to predict relative chloride diffusion coefficient by combining the effect of both water saturation degree and pore structure characteristics. The predicted results are validated against experimental data, and a concise analytical equation is proposed to predict the relative chloride diffusion coefficient. The equation indicated that the relative chloride diffusion coefficient is proportional to water connectivity but inversely proportional to the square of water tortuosity. Besides, the lattice model's quantitative results reveal that the water connectivity and water tortuosity are highly related to pre-water loading processes, and influenced by the gel pore fraction, which in turn will affect the relative chloride diffusion coefficient. Compared with existing equations and non-redistributed models, the present model could improve the prediction accuracy significantly.

1. Introduction

Chloride-induced corrosion of reinforcing steel is considered as the main deterioration of reinforced concrete (RC) structures exposed to marine and underground environments, and remains a hot topic related to concrete structural durability [1–4]. Although various driven forces can contribute to the chloride transport in cementitious materials (i.e., diffusion [5,6], migration [7,8], and convection [9,10]), diffusion driven by the species concentration gradient is one of the most fundamental chloride transport types [11]. For cementitious materials, the chloride diffusion coefficient is a major indicator for evaluating durability and an essential input parameter for the service life prediction model [12,13]. As a result, it is important to determine the chloride diffusion coefficient of cementitious materials accurately.

The chloride diffusion coefficient in cementitious materials highly depends on cementitious materials' pore structure characteristics and heterogeneous microscopic features [14,15], such as porosity, pore size distribution, connectivity, and tortuosity [16]. For saturated cementitious materials, the effects of pore characteristics on chloride diffusion have been well documented [17–19]. Page et al. [15] in 1981 observed that the chloride diffusion coefficient in saturated coefficients almost linearly increased with increasing total porosity. Tang and Nilsson [20] proposed an approach correlating the profiles of total chloride content to pore size distribution. An investigation in the previous work [21] also

* Corresponding author at: State Key Laboratory of Ocean Engineering, School of Naval Architecture, Ocean & Civil Engineering, Shanghai Jiao Tong University, Shanghai, China.
E-mail address: liuqf@sjtu.edu.cn (Q.-f. Liu).

https://doi.org/10.1016/j.cemconres.2023.107351
Received 24 March 2023; Received in revised form 29 September 2023; Accepted 16 October 2023
Available online 7 December 2023

found that treating the chloride diffusion coefficient as a function of pore size distribution could highly improve the predicting accuracy. Neithalath and Jian [22] confirmed that pore connectivity had a higher impact on ionic transport. Hornain et al. [23] found that increasing tortuosity could be attributed to the reduction of chloride diffusion. However, due to the alternate wetting and drying cycles by tidal and splash, or by seepage of groundwater, cement-based structures in practical environments are seldom absolutely dry or saturated. In partially saturated cementitious materials, the relative chloride diffusion coefficient D_{rc} has often been used to describe chloride diffusion. It is defined as a ratio of chloride diffusion coefficient at a specific saturation degree to that at the saturated state. In the analytical investigation, a few previous works have contributed to quantifying the relative chloride diffusion coefficient with relative humidity (*RH*). For example, Saetta et al. [24] described D_{rc} as an *S-shaped* function of *RH*:

$$D_{rc} = \frac{D(RH)}{D(RH = 100\%)} = \left[1 + \frac{(1 - RH)^4}{(1 - RH_c)^4}\right]^{-1} \quad (1)$$

where RH_c is a predefined critical relative humidity at which $D_{rc} = 0.5$, and it was defined as 75 % in Saetta's work. However, the previous studies indicated that RH_c is not a constant but may vary widely depending on temperature and pore structure [25,26]. Nielsen and Geiker reported a different value of RH_c as 83 % [25]. By adopting different RH_c, the predicted D_{rc} can be significantly influenced. Moreover, Eq. (1) is actually semi-empirical and cannot present specificities of microstructure because materials with the same *RH* may have different D_{rc} in a partially saturated system. Further investigation is needed to improve its accuracy. Except for relative humidity, some empirical equations were proposed with the saturation degree. Based on the measurements of ionic diffusion in masonry materials, Buchwald [27] related D_{rc} to the *S* and proposed an empirical power equation:

$$D_{rc} = \frac{D(S)}{D(S = 100\%)} = S^{\lambda} \quad (2)$$

where λ is a fitting parameter, which is found as 6 by Baroghel-Bouny et al. [28] and 4.5 by Olsson et al. [29]. Nevertheless, the above two equations do not fully account for the differences in pore structures of different cementitious materials as features of water-filled pores are not considered. In the unsaturated condition, only water-filled pores can act as transport medium for ionic diffusion while gas-filled phases will block the diffusion channels at the unsaturated state. Thus, even though the porosity, pore size distribution and the saturation degree are the same, ionic diffusivity of unsaturated materials could vary a lot due to different connectivity and tortuosity of water-filled transport channels [30,31]. Therefore, it is essential to investigate the chloride diffusion coefficient by taking into account the influence of both saturation degree and pore structure characteristics, especially water connectivity and tortuosity, which are also more challenging to be experimentally determined than porosity and pore size distribution [32,33].

Compared with the saturated state in which the pore structure effect has been widely considered, increasing but still limited work gave the quantitative analysis on the chloride diffusion considering unsaturated pore structure characteristics. Recent years, appreciating the development of computational technology, numerically modelling the ionic diffusion in unsaturated porous materials has received more attention by many scholars [34], in which the virtual microstructures are generally generated and the relationship between pore structure characteristics and ionic diffusivity can be directly determined [13,35,36]. For example, Martys [37] studied the effect of *S* on the ionic diffusion coefficient in two classes of sphere porous materials composed of overlapping and non-overlapping spheres. Based on a diffusive lattice network, a multicomponent lattice Boltzmann model (LBM) was used to model the phase separation of liquid and gas. However, this model is only available for the liquid-gas mixture with a density ratio of <58, which means the water-gas system with a density ratio of 1000 kg/m^3/1.29 kg/m^3 $\approx$ 775 is beyond the capacity. To overcome the drawbacks, a modified Shan-Chen LBM was proposed by Zhang et al. [38–40] based on the regenerated microstructure by combining the equation of state (EOS) and introducing the virtual density of the wall into the original Shan-Chen model. The effective porosity and water connectivity of the unsaturated system on D_{rc} were also discussed. He suggested a quadratic polynomial equation with three empirical constants a, b, c:

$$D_{rc} = \frac{D(S)}{D(S = 100\%)} = a \cdot S^2 + b \cdot S + c \quad (3)$$

However, it was reported that de-percolation of capillary pores in microstructures generated by the conventional growing sphere cement hydration models won't occurs until the porosity decrease to 4 % while a gradual de-percolation in the real microstructure starts at 40 % porosity, leading to the overestimation of the predicted ionic diffusivity compared with experimental data [41]. To overcome the drawbacks, Perko et al. [42] firstly proposed an improved growing sphere model which can provide a good match between the pore de-percolation value (50 %) with real materials by introduction a hollow shell mode of hydration. But the authors also state that further research of this model is needed to better match the connectivity of modelled and experimentally tested capillary pores at different porosities. In addition to the capillary pores, it has been demonstrated that the contribution of gel pores in C-S-H gels to water saturation and chloride diffusivity in unsaturated concrete is significant and cannot be ignored [43–45]. Although, some multiscale models were proposed to thoroughly investigate the hierarchical microstructure of partially saturated concrete on its ionic diffusivities by adopting computational homogenisation methods [46,47]. However, the pore structure characteristics of unsaturated concrete, which should also consider its microstructural features at multiscale, have yet to be investigated in their studies. The methodology to transform pore structure characteristics of gel pores at micro-scale to mesoscale is also unclear [48].

In addition to pore structure, chloride diffusion coefficient also depends on the water distribution of pore structure. In an atmospheric environment, the cement-based materials may undergo arbitrary drying-wetting cycles, leading to water distribution changes in the pore structure. Cyclic drying-wetting processes and the initial pore structure are fundamental factors influencing the water distribution and have to be further considered to predict the D_{rc} value. However, to the best of the authors' knowledge, there is no numerical study that considers both water saturation degree and pore structure to propose a prediction model for the relative chloride diffusion coefficient and takes into account the effect of arbitrary drying-wetting cycles on water distribution and pore structure characteristics.

In this study, a numerical study is carried out to propose a novel lattice model to investigate the ionic diffusivity in unsaturated cementitious materials accounting for its hierarchical microstructures. Firstly, the chloride diffusion process in unsaturated cementitious materials will be thoroughly introduced. Subsequently, 3D representative volume elements (RVEs) of C-S-H gels and cement paste will be numerically generated. To avoid the inaccuracy of traditional grow-sphere hydration model and to match the capillary porosities of real materials at which de-percolation starts and ends, a redistribution process was applied to the capillary pores of the initial pore structure, and can provide a good match between connectivity of modelled and real microstructure at different porosities. Based on the redistributed RVEs, water distributions in pore structures at various saturation degrees, including gel and capillary pores, are simulated with the consideration of different drying-wetting processes. By converting the unsaturated RVEs into diffusive lattice networks, the relative chloride diffusion coefficients with different *S* will be predicted and validated against experimental results. Combining predicted relative chloride diffusion coefficients and pore structure features computationally extracted at multiscale, a pore structure-dependent equation for describing the D_{rc}—*S* relationship is

established. The existing and present model are also compared to evaluate the accuracy of the proposed model, and the underlying mechanisms of chloride diffusion in unsaturated cementitious materials are also discussed in depth.

2. Chloride diffusion in unsaturated cementitious materials

Compared with cement paste, which contains a pore structure, aggregates and sands can be treated as impermeable composites during the chloride diffusion in concrete [33,49]. Thus, to investigate the intrinsic transport properties of concrete from a microscopic perspective, the representative volume element (RVE) of cement paste is selected, as shown in Fig. 1.

As presented in Fig. 1(a), typical pores in cement paste have a wide range of sizes, including C-S-H gel pores, small capillary pores, and large capillary pores [12,50]. Except for capillary pores, gel pores also play a critical role in the ionic diffusion process and cannot be ignored [44,51,52]. Therefore, the pore-scale investigation of chloride diffusion should take into account the effect of different pore-size groups. Besides, in most environmental conditions, cement paste is commonly unsaturated owing to the complex water loading history, such as alternative drying-wetting cycles and cyclic atmospheric conditions, as displayed in Fig. 1(b). Compared with the saturated state, the chloride transport process in unsaturated cement paste becomes more complex, and chloride diffusion coefficient varies at different saturation degrees as $D_{cl}(S)$. At specific saturation degree (S), $D_{cl}(S)$ can be expressed as $D_{rc}(S) \times D_{cl0}$. $D_{rc}(S)$ is the relative ionic diffusion coefficient, which is defined as the ratio of current diffusivities in the unsaturated state to the diffusivity in the saturated state (D_{cl0}). $D_{rc}(S)$ ranges from 0 to 1; generally, D_{cl0} can be predicted by many analytical or numerical methods [12].

Due to the different shapes of pores, the water distribution in unsaturated pore structures will be affected according to the so-called ink-bottle or pore throat effects [32,53]. As shown in Fig. 1(c), compared with the saturated condition, in which the pore structure is fully saturated with water and can be treated as effective diffusion path for chloride, some pores are occupied by the gas phase in unsaturated porous systems, and the water-filled pores (diffusion path) are partially continuous or partially discontinuous. Therefore, except for saturation degree (S), the chloride diffusion coefficient in unsaturated cementitious materials is highly dependent on various characteristics of pore structure, such as water tortuosity ($\tau(S)$), water connectivity ($\eta(S)$) and water-saturated porosity. Water tortuosity is the ratio of the shortest distance that ions or molecules must travel to a direct distance in the diffusion direction at an unsaturated state [33]. The water connectivity presents the connected water fraction in unsaturated pore structure [54,55]. At different saturation degrees (S), the water tortuosity ($\tau(S)$) and water connectivity ($\eta(S)$) of the transport channels vary. From the microscopic perspective, $D_{rc}(S)$ should be analysed with different pore structure characteristics, which however are affected by water distribution in capillary and gel pores according to the water loading processes.

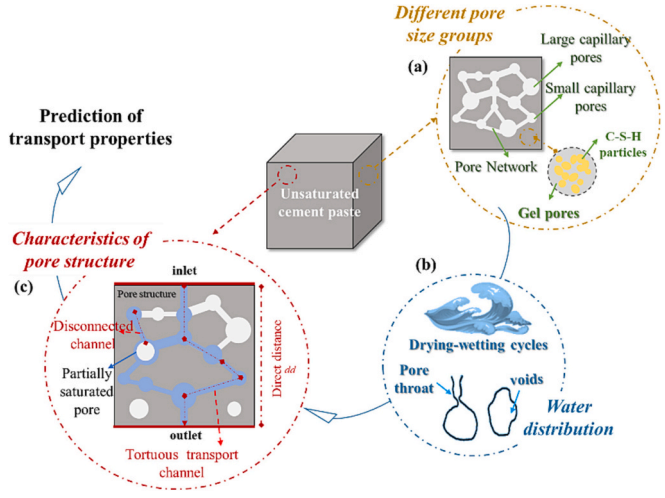

Fig. 1. Representative volume element (RVE) of cement paste.
(a) Different pore-size groups (b) Water distribution considering pore shapes (c) Illustration of pore structure characteristics.

Therefore, the following sections propose a novel lattice model to improve the prediction accuracy of the chloride diffusion in unsaturated cement paste. Fig. 2 illustrates the modelling procedures. As present in Fig. 2(a), to investigate the transport properties of cement paste considering its hierarchical microstructures, RVEs of different levels are developed in Section 3. A novel redistributed lattice model is proposed to better represent the de-percolation phenomenon of capillary pores, which influence the transport channels significantly. In Section 4, given that D_{rc} is closely related to the water distribution at the unsaturated state, by taking into account the pore throat effect in gel and capillary pores, repeated drying-wetting cycles are simulated to model the water distribution of pore structure in C-S-H gels and cement paste as shown in Fig. 2(b). With the help of computer-based methods, pore structure characteristics at different levels are determined in Section 5 (Fig. 2(c)). Then, Section 6 introduces a lattice diffusive network based on the novel redistributed RVEs to predict the relative chloride diffusion coefficient under different saturation degrees. The predicted results are compared with experimental data obtained from the literature (Fig. 2(d)). Based on the quantitative pore structure characteristics, the relationships between pore structure and chloride diffusivity in unsaturated cementitious materials and the effect of water distribution on chloride diffusivity are further analysed in Section 7, as listed in Fig. 2(e). A concise prediction equation for the relative chloride diffusion coefficient is also put forward based on the quantitative data. Besides, the proposed model is also compared with existing equations and models in Section 7.

3. Modelling of representative volume elements at different levels

As illustrated in Section 2, except for capillary pores, the contribution of gel pores in C-S-H gels to ionic diffusivity in cementitious materials cannot be ignored. Herin, in this section, the 3D representative volume elements (RVEs) of both C-S-H and cement paste are simulated. To better match the de-percolation effect of capillary pores in hardened cement paste, a novel redistributed lattice model is proposed.

3.1. C-S-H level

Based on previous literatures [12,56,57], C-S-H gel can be classified into two types according to their porosity: the high-density (HD C-S-H) gel in the inner layer C-S-H layer and the low-density (LD C-S-H) gel in the outer layer. Following the results reported by Ulm et al. [58], Constantinides and Ulm [43], the gel porosity of these two C-S-H gels are determined as:

$$\varnothing_{HDCSH} = 0.24 \text{ and } \varnothing_{LDCSH} = 0.37 \quad (4)$$

To generate the desired RVEs of C-S-Hs with defined porosities, the take-and-place algorithm reported by [47,59] was adopted. The individual C-S-H particle was assumed to be a sphere with a diameter of 5 nm with an impenetrable hardcore surrounded by a softshell. During the generation process, the soft shell of a newly introduced C-S-H particle can overlap freely with soft shells and hard cores of other existing C-S-H particles. To model the C-S-H growing phenomenon [60], the hard core of a new particle should overlap with the softshell of existing C-S-H particles but leave any hardcore of existing particles non-overlapped. According to Liu et al. [59], the size ratio between the soft shell and hard core was set as 3:2. Nano-crystal hydrates are considered as a part of C-S-H particles and the RVE sizes of both HD and LD C-S-H were set as

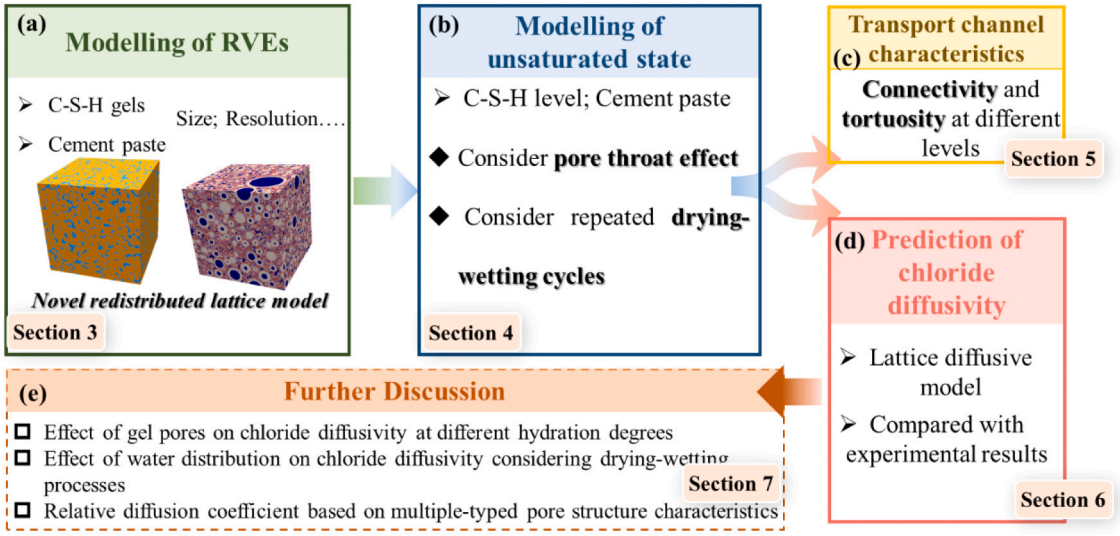

Fig. 2. The flowchart of the modelling procedure.

$100 \times 100 \times 100 nm^3$ with resolution of 0.5 nm/voxel according to [61,62]. Typical microstructures of HD and LD C-S-H gels are shown in Fig. 3. The pore structure of LD C-S-H gel with higher porosity, which is illustrated by blue areas, shows a more porous structure compared with HD C-S-H. The gel pore radius of these two kinds of C-S-H gels ranges from 1 nm to 5 nm, comparable to 2.5-5 nm reported in [63,64].

3.2. Cement paste levels

Various computer-aided technologies are proposed to obtain cement paste's 3D microstructure, such as computer-based models and X-ray computed microtomography techniques. Among them, several helpful software is widely used, e.g. CEMHYD3D, HYMOSTRUC3D and μic. With the μic platform, users can model the microstructural development by defining materials, particles and reactions, and the hydrated cement clinkers will be modelled as coated layers [12,46]. In this study, the cement hydration process is coded through XML files and run through the μic platform, which is highly customisable. A more detailed platform introduction can be found in [65]. Previous literature has provided many comparisons between modelled results by the platform and by experiments on hydration properties such as hydration degree (α) and volume fraction of hydration products, showing an acceptable accuracy [66,67]. A schematic illustration of simulated RVE at the cement paste level is shown in Fig. 4(a).

However, as a kind of particle-based cement hydration model, it was reported that the connectivity of the capillary pore structure modelled by it would be too high [36,41], leading to the significant over-estimation of diffusivity in the cementitious materials. To avoid this inaccuracy and to match the capillary porosities of real materials at which de-percolation starts and ends, this study proposed a novel redistributed lattice model (inspired by [42,68]) by redistributing the capillary pores in the original RVEs simulated by the μic platform. Through this, the "real" pore structure of hardened cement paste can be better represented by the redistributed RVEs. Specific processes are as follows. According to the research done by Achour et al. [12] and Ma et al. [69], the capillary pores can be divided into small and large capillary pores, where smaller groups can be regarded as embedments in outer hydration products (generally including crystals and LD C-S-H). The porosity of small capillary pores can be estimated by an empirical equation [69]:

$$\varnothing_{SCP} = \frac{0.712\alpha - 0.255\frac{\alpha^2}{w/c}}{\left(0.37 + 0.226\frac{\alpha}{w/c}\right)(1 + 3.15w/c)} \tag{5}$$

Based on this proportion, the original capillary pores can be redistributed. As shown in Fig. 4, the voxel presenting small capillary pores will be randomly selected and embedded into the outer layers individually. The replaced voxel in the outer layer will then be relocated to the pore network and substitutes pore voxel. During the process, the volume fraction of both capillary pores and hydration products remains

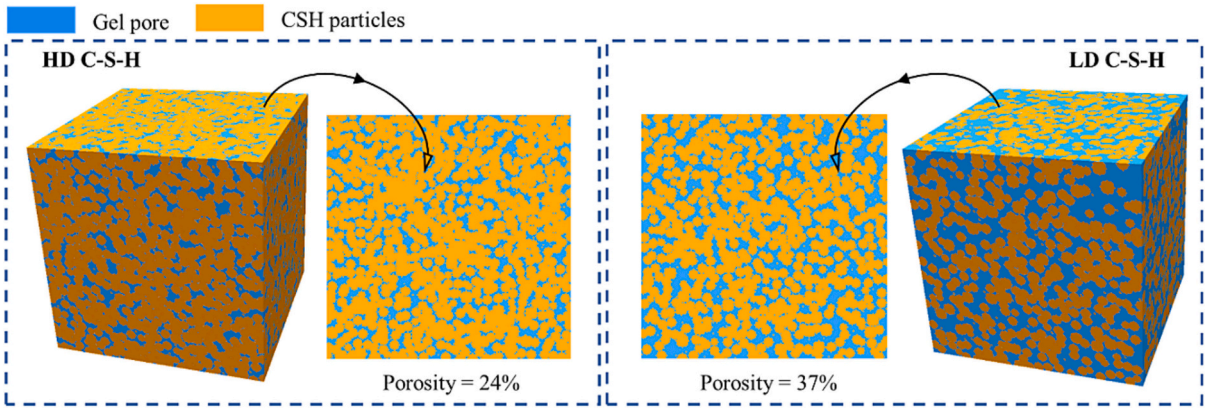

Fig. 3. Typical microstructures of HD and LD C-S-H gels.

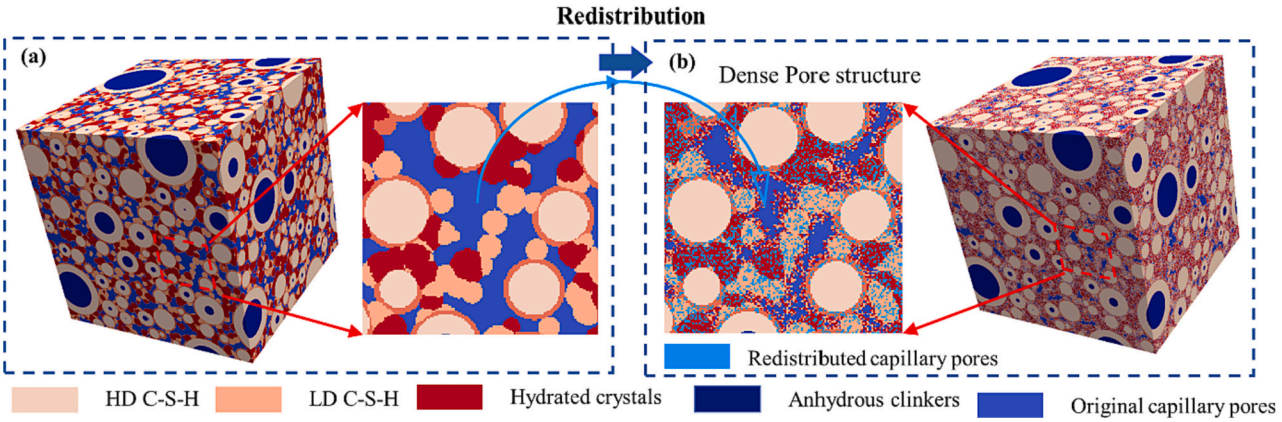

Fig. 4. A schematic illustration of the redistribution process of original RVEs. (a) Original RVE (b) Novel redistributed RVE.

constant. This procedure will continue until the porosity of redistributed capillary pores equals the porosity calculated by Eq. (5). Besides, it should be noted that the new positions which hydration product voxels removed to should have at least one surface connected with other existing hydration products voxels. Otherwise, the outer layer will be completely dispersed, and the embedding phenomenon will disappear. After the redistribution process, it can be seen pore structure of the original capillary pores (the area shown by dark blue) in Fig. 4(b) is obviously denser compared with Fig. 4(a).

Regarding RVE size, as indicated in [70], the minimum size for determination of diffusivity in cement paste is 100 × 100 × 100 μm^3. Accordingly, the cubic size of cement paste was chosen as 100 × 100 × 100 μm^3 in this study. A continuous cement particle size distribution with a minimum size of 1 μm and a maximum size of 50 μm is used [38]. The curing temperature is defined as 293 K. The cement used for modelling is Portland cement CEM I 42.5 N, and its mineral phase mass ratios are $m_{C_3S} = 0.6353, m_{C_2S} = 0.13, m_{C_3A} = 0.0843, m_{C_4AF} = 0.09$, $m_{Gypsum} = 0.0117$ which is provided in [26,38]. To better present the depercolation effect of capillary porosities, the resolution of RVE at the cement paste level is elected according to the comparison of the modelled connected fraction of capillary pores with different resolutions and natural material reported by Bentz et al. [71,72]. Fig. 5(a) shows the connected fraction of capillary porosity in redistributed RVEs with four different resolutions (1, 0.5, 0.4, 0.25 μm/voxel) at three capillary porosities (0.25, 0.3, 0.4). As the resolution accuracy increases, the connected fraction of capillary pores rises, consistent with the finding reported in [39,40]. Selecting the resolution of 0.5 μm/voxel, it can be seen in Fig. 5(b) that there is a good match between the calculated fraction and data reported by Bentz et al. Fig. 5(b) also illustrated that the redistribution process enables a more accurate spatial distribution of capillary pores compared with the original simulated RVEs. Based on the modelled results, the resolution of 0.5 μm/voxel will be adopted in this study, which is the same as that employed by Zhang et al. [38] and Lin et al. [73]. Besides, it should be noted that only the conception that small capillary pores are embedded in hydration products is considered, the actual pore size of small capillary pores is not clarified due to the limitation of resolution.

After determining the size and resolution of RVEs, Fig. 6 showed the simulated microstructure of cement paste at three hydration degrees with 0.50 *w/c*. With the increased hydration times, the pore structures become denser. It can also be seen that the generated microstructure is

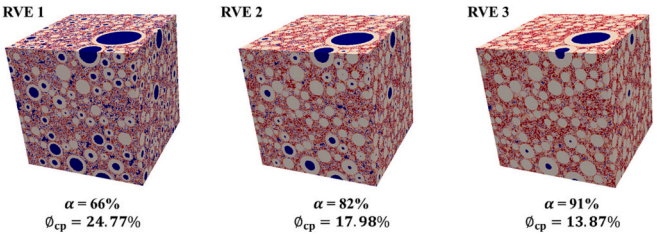

Fig. 6. RVEs of hardened cement pastes at three different hydration degrees 100 × 100 × 100 μm3, 0.5 μm/voxel, *w/c* = 0.5.

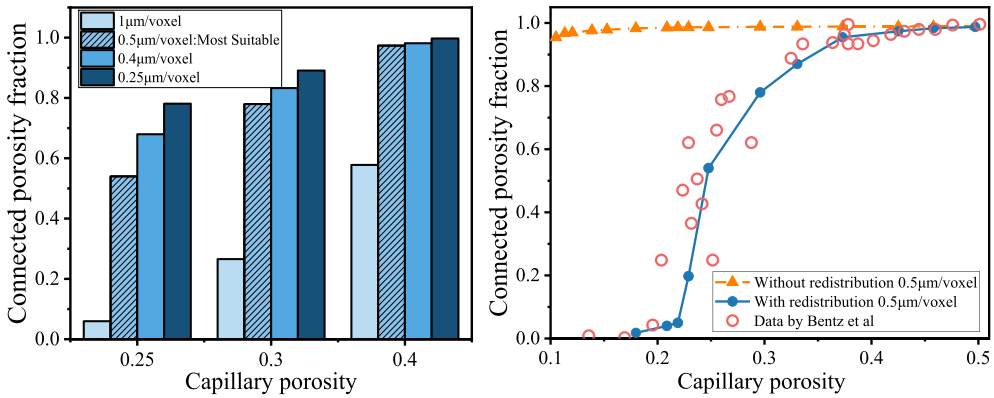

Fig. 5. Connected porosity fraction at different capillary porosity.

an assemblage of pores, anhydrous particles and solid hydrated products. After seven days of hydration, the hydration degree reaches 66 %, consistent with the experimental data reported in [69] as 67 %. As the hydration process evolves, the pore structure is condensed by the solid hydration products. The capillary pores are seldom connected when the hydration degree increases from 66 % to 91 %, as displayed in Fig. 5(b). In this situation, the transport channels may transform from the connected capillary pores to the serial connections of capillary pores entrapped by gel pores [42], which will be analysed later. This also indicates the importance of considering gel pores' effect during the diffusivity prediction in cementitious materials.

4. Modelling of unsaturated water distribution at different levels

Due to the alternative drying-wetting cycles in the atmospheric environment, cementitious materials are often unsaturated. At this stage, water distribution in unsaturated pore structure, which is influenced by a wide range of pore groups, including gel and capillary pores, can play a critical role in determining ionic diffusivity. This section will simulate the 3D water distribution in unsaturated C-S-H gels and cement paste using a computer-aided technology based on the redistributed saturated RVEs obtained in Section 3. The dynamic water loading history and the water trapping effect were also considered.

4.1. Modelling procedures of single wetting and drying process

4.1.1. C-S-H level

Compared with gel pores, the solid C-S-H particles can be regarded as an impermeable phase at the C-S-H level. At the unsaturated stage, it is reported that the pore structure characteristics, such as pore size distribution and pore throat, will influence the water distribution [32,74]. Thus, it is reasonable to first analyse irregular pore structure's pore size before modelling the water distribution at different saturation degrees [75]. Taking LD C-S-H as an example, Fig. 7(a) shows the pores of the reconstructed C-S-H gels by using the pore size extraction method (largest sphere method) [76–79]. Here, the application procedure is briefly listed as follows. Firstly, the shortest distances of any voxel in the pore space from the solid wall are marked to form a distance map. Secondly, the marked number for each pore voxel is selected as the radius of the sphere, which is centralised on the voxel. Through this, the pore space can be regarded as a connection of different sizes of pores, as shown in Fig. 7(b). All these spheres just touch the edge of the solid, and the overlapping areas between larger and smaller spheres are considered to belong to larger spheres. Finally, the largest sphere is obtained for each voxel, and the pore size can be extracted. More details can be found in the author's latest work [21].

After determining the pore size distribution by the largest sphere method, the water filling/wetting procedure in a porous medium can be modelled by the pore geometry method, which assumes the filling procedure is only dependent on the pore network of the porous materials without any pre-set parameters [80–83]. During the single water-filling process, according to the Kelvin-Laplace eq. [64,84,85], the water adsorption in the pore structure is solely dependent on the pore size in the case of idealised moisture distribution. Only the pore radius smaller than a critical pore diameter d_c can be filled at a specific relative humidity. With the increase of relative humidity (the filling process) from the inlet surface, the water phase will fill the pore structure from smaller to larger pores until a pre-defined water saturation degree S is reached, as illustrated in Fig. 7(c).

However, as schematically illustrated in Fig. 8, desorption can result in water trapping because of the small pore blocking. Fig. 8(a) shows the saturated channel consisting of two kinds of pore groups (diameter d_1 and diameter d_2, $d_2 > d_1$). At specific conditions, if the critical pore size is d_1, Fig. 8(b) shows a desorption process, the larger pores d_2 at two ends (Part A and Part C) can be drained. However, the medium part B is trapped by the small pores. In this situation, the pore group with diameter d_1 is not totally drained, and the water trapping effect will strongly influence the water tortuosity ($\tau(S)$) and water connectivity ($\eta(S)$) of transport channels at specific saturation degrees. In the present

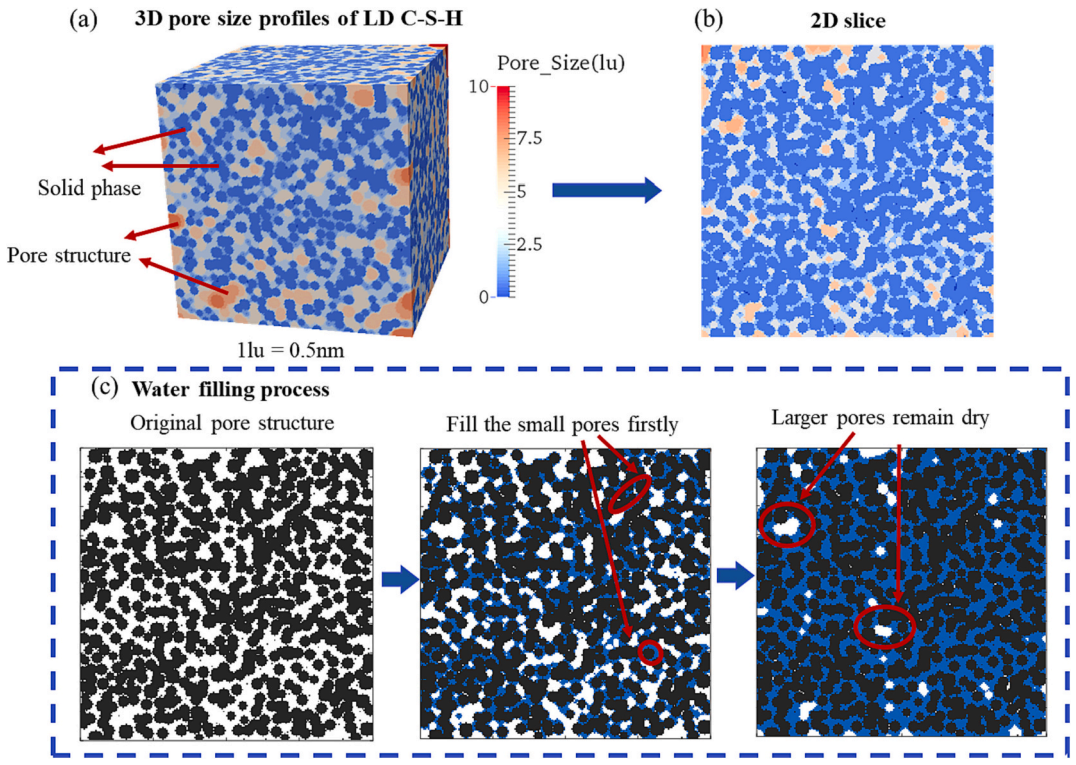

Fig. 7. Schematic illustration of the water-filling process at the C-S-H level.
(a) Pore size of gel pores (labelled by lattice units, lu, 1lu = 0.5 nm) (b) 2D slice (c) water filling process in LD C-S-H.

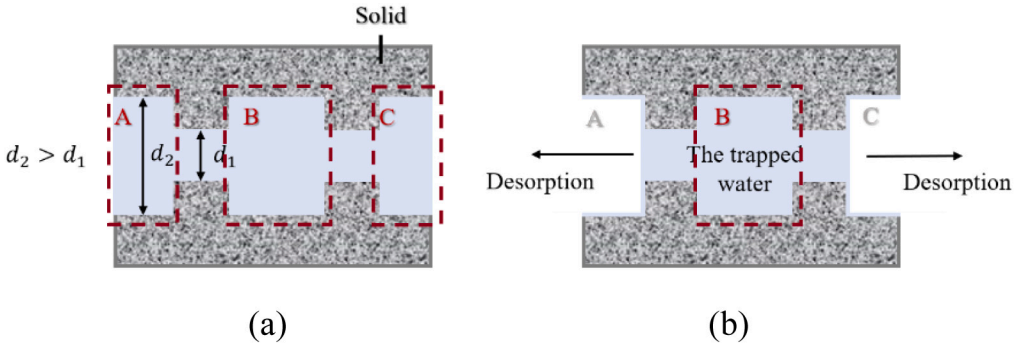

Fig. 8. The illustration of the drying process at C-S-H level (a) saturated (b) drying.

study, considering that the surface water is located within <1 nm and strongly bound to the surface of the C-S-H layer, the thin water film is neglected due to the current resolution limitation. The difference reported by Cohan et al. [86] in critical pore radius and meniscus between the drying and wetting processes is also not distinguished, as this paper focused on the order of pore size during adsorption or desorption procedures. The criterion for completing the wetting or drying procedure is whether the desired saturation degree is reached.

4.1.2. Cement paste level

At the cement paste level, except for large capillary pores, redistributed small capillary pores (which are "embedded" into LD C-S-H) and gel pores in LD/HD C-S-H should be considered together when modelling the water distribution at unsaturated conditions. Still, following the Kelvin-Laplace equation, the single wetting process of cement paste will gradually fill the pore structure, following an order from gel pores in LD/HD C-S-H to small/large capillary pores. This filling method has been successfully used to investigate the saturation-related properties of concrete considering hierarchical pore structure, e.g., water sorption isotherm [61] and water permeability [87]. But, in the drying procedure, the water-trapping effect should be considered, and the drying process can be divided into three steps, as shown in Fig. 9.

In the first step, from the surface exposed to the surrounding environment, connected capillary pores will dry firstly from larger to small pores until all the remaining water-filled capillary pores are trapped by C-S-H gels, as shown in Fig. 9(a). Then in the second step, the C-S-H gels, next to the gas-filled pores or C-S-H voxels under threshold saturation degree, begin to dry. The present study defines a threshold when a gas-filled pore is percolated in LD/HD C-S-H gels (Fig. 9(b)), and connected gas-filled channels can provide releasing channels for trapped water. When the saturation degree of the C-S-H voxel is below the threshold, adjacent voxels, including water-filled capillary pores or C-S-H gels, can release water through this channel, as shown in Fig. 9(c). In the third step, the RVEs will repeat step two and keep drying until the defined saturation degree is achieved.

4.2. Setting of drying-wetting cycles and model results

After introducing a single drying-wetting process at C-S-H and cement paste levels, alternative drying-wetting cycles are applied to obtain the desired water distribution in the pore structure. At the cement paste level, to get stable results and reduce the impact of random water distribution on the chloride diffusivity prediction caused by arbitrary water loading cycles, water distribution in RVEs of cement paste was modelled as relatively uniform in the present study. Initially, the RVEs are set as saturated, and then the drying-wetting cycles of cement paste are randomly chosen until the saturation of each slice is within a limited range. Fig. 10 displays the saturation degree of each slice in modelled RVEs corresponding to that shown in Fig. 6. In the present study if the aimed saturation degree is S, the upper limit is $S + 0.05$, while the lower limit is set as S - 0.05. Through this, the water saturation in each slice of RVEs is generally uniform. The stability of this uniformly distributed method will be discussed with pore structure characteristics in the next section, and the effect of unevenly distributed water on cement paste's transport properties will be later analysed in the discussion section.

However, the relatively homogeneous water distribution is no longer applicable at the C-S-H level. Although the water distribution of cement

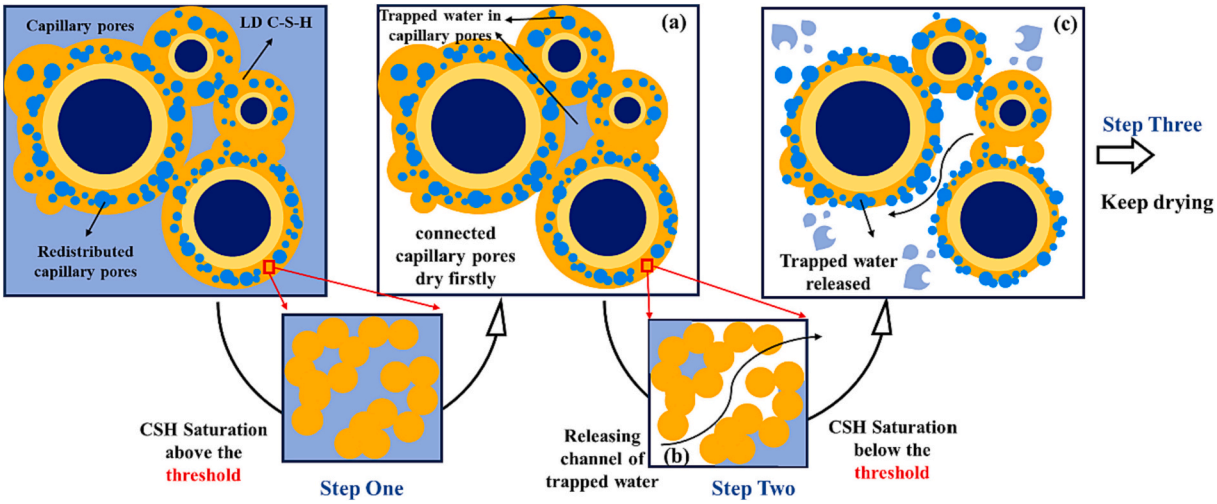

Fig. 9. Schematic illustration of the water-drying process at cement paste level.

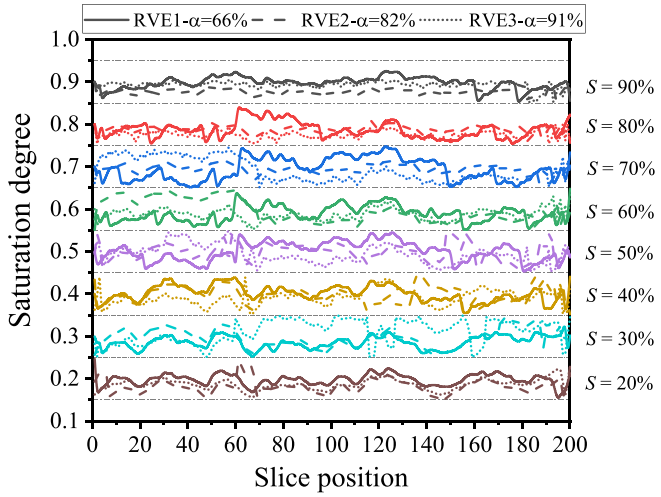

Fig. 10. Water distribution of different slices.

paste is uniform, the water distribution in each HD/LD C-S-H voxel is hard to determine. Even though the saturation degrees of different voxels are known, the applied drying-wetting cycles are unclear and may strongly affect the transport properties [74]. To solve the problem, 20 RVEs are generated for HD and LD C-S-H, respectively. For each RVE, water distributions of gel pore structure at 9 saturation degrees (100 %, 90 %, 80 %, 70 %, 60 %, 50 %, 40 %, 30 %, 20 %) are modelled. 10 randomised cyclic drying-wetting loops for each saturation degree. In total, $20 \times 2 \times 9 = 360$ different 3D RVEs with different saturation degrees or water distributions were simulated. Fig. 11 shows one of the modelled water-gas distributions in the C-S-H gels. It can be seen that water tends to cover the C-S-H surface and fill the small pores, while gas tends to fill the large pores and form the gas clusters. This finding is also consistent with the modelled results done by [47,78]. Besides, as demonstrated by HD C-S-H at 30 % saturation, it can be found that due to the random drying-wetting cycles, the water distribution among different slices is not uniform compared with cement paste.

Based on the data obtained from these 360 RVEs, the prementioned threshold of the releasing channel is set as 0.8 and 0.5 for LD and HD C-S-H respectively (detailed data can be found in Appendix A: Fig. A.1). Fig. 12 shows the modelled water-gas distributions of cement paste at saturation 90 %, 60 % and 30 %, RVE1 with *w/c* ratio 0.5 and hydration degree 66 % are taking as an example. As displayed in 3D microstructures (Fig. 12(a-1,2,3)), gas tends to form clusters in the pore structure with decreasing water saturation. At this stage, the water-filled capillary pores may be trapped by the gel pores in C-S-H gels, and the transport channels become serial connections of capillary pores linked by water-filled C-S-H matrixes [83]. 2D slices can illustrate the three drying steps clearer and show the trapped water. As seen at the saturation of 90 % (Fig. 12(b-1)), the C-S-H gels remain saturated and capillary pores gradually lose their water. When saturation drops to 60 %, as shown in Fig. 12(b-2), the C-S-H begins to dry, but the threshold is not reached. Thus, some water is trapped in the redistributed capillary pores, as highlighted in red in Fig. 12(c-1). When the saturation keeps decreasing to 30 % (Fig. 12(b-3) and Fig. 12(c-2)), the trapped water is released, and the C-S-H matrix also loses its water. The inhomogeneous water distribution in the C-S-H matrix shown in Fig. 12(c-2) also informs the necessity of stochastic modelling of drying-wetting processes at the C-S-H level.

5. Determination of pore structure characteristics at different levels

As a typical porous material, chloride diffusivity of unsaturated cementitious materials is highly dependent on various characteristics of pore structure, such as water tortuosity (τ), water connectivity (η) and water-saturated porosity. In this section, water tortuosity ($\tau_{CSH}(S)$, $\tau_{Paste}(S)$) and connectivity ($\eta_{CSH}(S)$, $\eta_{Paste}(S)$) of both C-S-H and cement paste at different saturation degrees are determined. A multiscale computational homogenisation method is adopted to upscale the parameters from C-S-H to cement paste levels.

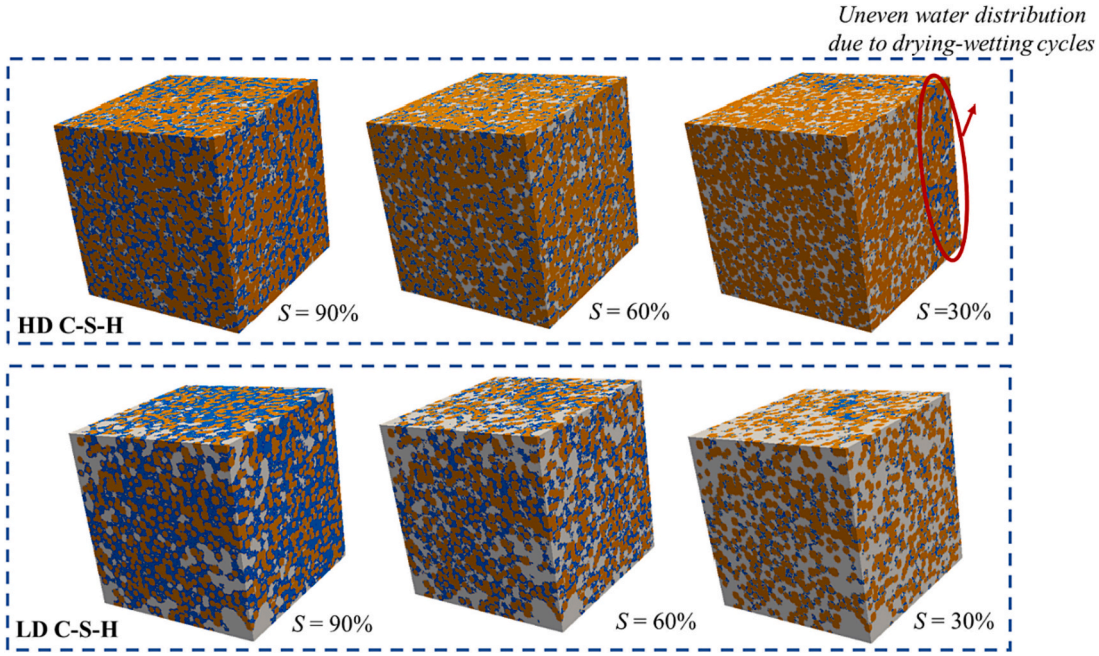

Fig. 11. Water-gas distribution in C-S-H gels.
(Bule, white, and yellow represent water, gas, and C-S-H particles, respectively). (For interpretation of the references to colour in this figure legend, the reader is referred to the web version of this article.)

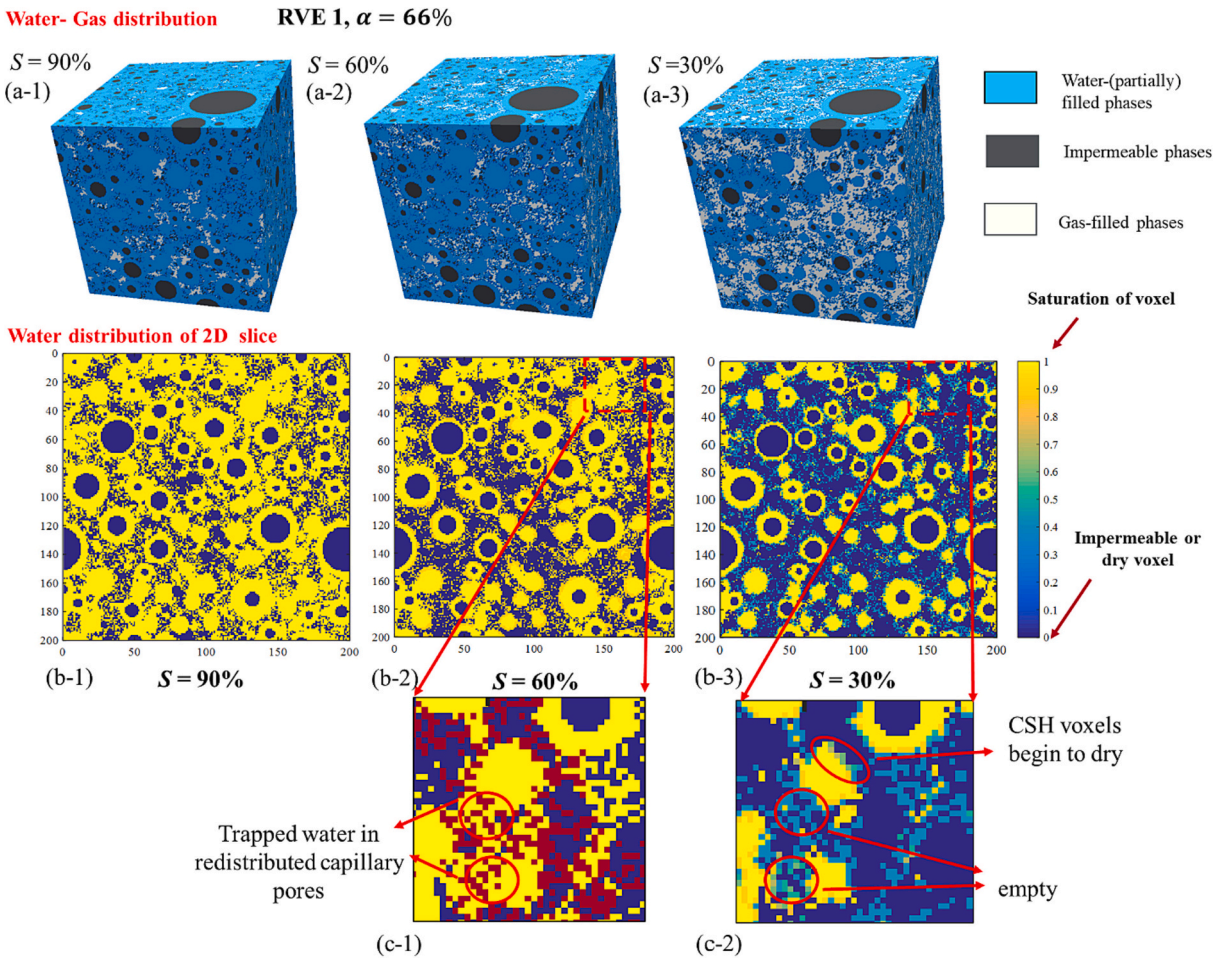

Fig. 12. Water- gas distribution in cement paste (RVE 1, α = 66%).
(a) 3D microstructure (b) 2D slices of saturation of voxels (c) The illustration of trapped water in capillary pores.

5.1. C-S-H level

Based on the simulated unsaturated C-S-H gels' RVEs, water tortuosity ($\tau_{CSH}(S)$) and connectivity ($\eta_{CSH}(S)$) at the C-S-H level can be quantified. As illustrated in Section 4, C-S-H particles can be considered as impermeable phases compared with gel pores. Therefore, from the inlet side to the outlet side, only connected water-filled gel pore voxels are available to form channels for chloride diffusion, as shown in Fig. 13 (a). For each pore voxel (orange cube), the connected voxels are defined as 6 face-to-face ones, and the voxel connectivity of each water-filled (η_v) voxel is defined as 1, while the voxel connectivity of gas-filled ones is defined as 0. Similar to the modelling procedures done by Zhang et al. [38], the water connectivity ($\eta_{CSH}(S)$) of the C-S-H gels at a specific saturation degree (S) is calculated by dividing the number of connected water-filled voxels by the total number of water-filled voxels. Generally, $\eta_{CSH}(S)$ is smaller than 1. $\eta_{CSH}(S) = 1$ indicates all the water-filled pores are interconnected. If the $\eta_{CSH}(S)$ is 0 but the S is non-zero, the water-filled pores in the domain are disconnected and randomly

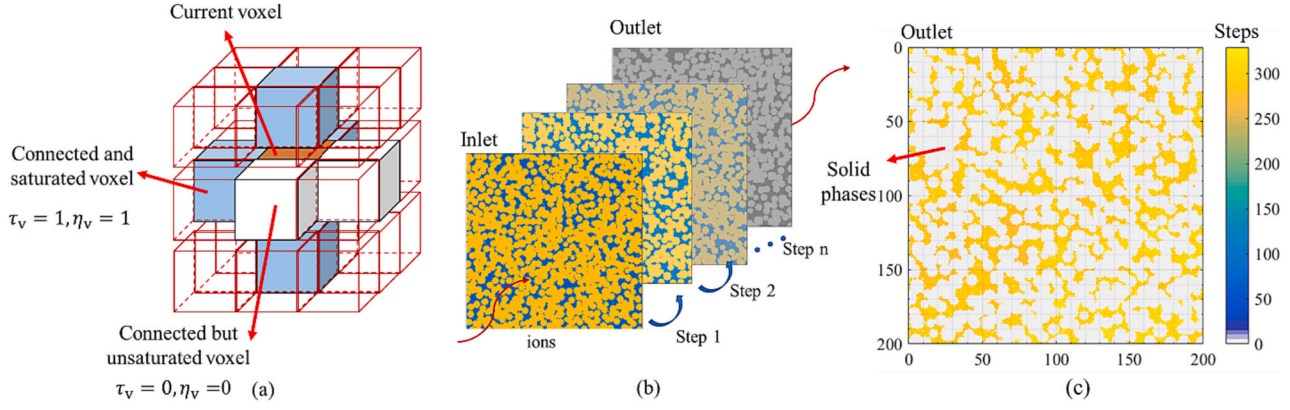

Fig. 13. Schematic illustration of the determination of pore structure characteristics.
(a) Connectivity (b) Tortuosity (c) Travelled distance of the outlet.

dispersed. The effective porosity of C-S-H ($\varnothing_{CSH}^{eff}$) which presents the connected fraction of water-filled pores, is calculated by multiplying the degree of water connectivity by the porosity of C-S-H and saturation degree, as $\varnothing_{CSH}^{eff} = \eta_{CSH}(S) \cdot S \cdot \phi_{CSH}$.

For the water tortuosity, as shown in Fig. 13(b–c), the steps travelled by ions from the inlet to the outlet can be computationally determined. For example, Fig. 13(c) shows the needed steps that ions diffuse through water-filled pores from the inlet to the outlet. It can be seen that the distance travelled by ions (>250 steps) is bigger than the lattice size of the sample (200). Therefore, the water tortuosity (τ_{CSH}) of the C-S-H gels at a specific saturation degree (S) is calculated by dividing the averaged steps of the outlet by the lattice size of the C-S-H sample. Generally, $\tau_{CSH}(S)$ is >1. If the modelled steps on the outlet are empty, it means that ions cannot diffuse through the sample, and the $\tau_{CSH}(S)$ is defined as infinity (∞).

Fig. 14 shows the extracted results of water connectivity and tortuosity in HD and LD C-S-H gels against saturation degree. Solid lines present the averaged values obtained based on the 360 RVEs applied to randomised cyclic drying-wetting processes, as illustrated in Section 4.2. Detailed results are provided in Appendix A. The results indicate that the connectivity of water-filled pores gradually decreased with the decrease of saturation degree in both HD and LD C-S-H. In contrast, the water tortuosity shows an opposite trend. Compared with LD C-S-H, the decreasing trend of water connectivity for HD C-S-H, which owns lower porosity, is more prominent. Besides, as circled in Fig. 14(a), the water connectivity decreases slightly within a specific range and drops sharply after a critical saturation degree. This is because water tends to fill smaller pores while the gas phase prefers to occupy the central part of larger pores. Only going down a critical saturation degree, the gas phase can form clusters and obstacle the diffusion pores, leading to a sharp drop in water connectivity [83]. Similarly, once the water saturation degree reaches the critical saturation degree, the gas clusters will block the diffusion path, resulting in a more tortuous water-filled pore structure. The water tortuosity will go up quickly.

The averaged values in Fig. 14 are also compared with the results determined based on the RVEs with uniformly distributed water (the dashed lines), and show relatively lower values in connectivity. According to the detailed results in Tables A1–A2, the connectivity of HD C-S-H with randomised cyclic process has higher fluctuations. It may even drop its connectivity to 0 even the saturation degree is 80 %. But the randomised results are stabler with larger porosity in LD C-S-H. Therefore, the difference shown in LD C-S-H is relatively minor. In the present study, the averaged values can consider the complex water loading history and present the local information. Thus, using the computational homogenisation method, the averaged value will be upscaled to the cement paste level.

5.2. Cement paste level

Basic procedures to find the connected voxels of the water- partially filled voxels by face-to-face searching at the cement paste level, including C-S-H voxels or capillary voxels, are similar to those illustrated at the C-S-H level. However, to calculate $\eta_{Paste}(S)$, the connectivity of each voxel (η_v) at cement paste should be classified as C-S-H ($\eta_v^{CSH}(S)$) and capillary pores (η_v^{cp}) as shown in Fig. 15. For C-S-H voxels with different saturation degrees, the connectivity η_v for C-S-H gels is no longer a constant value 1 but determined according to the averaged results $\eta_v^{CSH}(S)$ = averaged $\eta_{CSH}(S)$. At the cement paste level, the overall connectivity of the pore structure at a specific saturation degree (S) is calculated by the following equation:

$$\eta_{Paste}(S) = \frac{\sum_{i=1}^{i=n}\left(\eta_{v,i}^{CSH}(S_i) \times S_i^{CSH} \times \phi_{v,i}^{CSH}\right) + \sum_{i=1}^{i=N}\eta_{v,i}^{cp} \times \phi_{v,i}^{cp}}{\sum_{i=1}^{i=n}\left(\phi_{v,i}^{CSH}\right) + \sum_{i=1}^{i=N}\phi_{v,i}^{cp}} \quad (6)$$

where n, N are is number of connected C-S-H voxels and capillary pores voxels, respectively; $\eta_{v,i}^{CSH}(S_i)$ means the connectivity of water-filled gel pores in C-S-H voxels with saturation degree S_i; $\eta_{v,i}^{cp}$ is the connectivity of pore voxels, with value 1 for water-filled ones, 0 for gas-filled ones. $\phi_{v,i}^{CSH}$ is the original porosity of C-S-H voxels, which is 0.24 for HD C-S-H and 0.37 for LD C-S-H; $\phi_{v,i}^{cp}$ is the porosity of capillary pore voxel, and is set as 1. While $\eta_{CSH}(S)$ corresponds to the connected fraction of water-filled pores, it should be noted that $\eta_{Paste}(S)$ presents the connected fraction of pore structure and reflects the transport properties of pore structure.

Although the tortuosity ($\tau_{Paste}(S)$) is still calculated by dividing averaged steps of the outlet by the size of the cement paste sample, the step of each voxel is no longer 1 at C-S-H gels. It should be determined according to the results calculated at the C-S-H level. Similarly, $\tau_{Paste}(S)$ can be calculated by:

$$\tau_{Paste}(S) = \frac{\sum_{1}^{n_{outlet}} step_{v,i}}{n_{outlet} \times L_{size}} \quad (7)$$

where n_{outlet} is the number of connected voxels on the outlet surface; $step_{v,i}$ is the modelled steps similar to the Fig. 13(c), L_{size} is the lattice size of the sample, which is 200 in the present study.

Herein, the calculated connectivity and tortuosity of unsaturated cement paste at different saturation degrees are demonstrated in Fig. 16 (a). Compared with water tortuosity, which increased with increasing hydration degree, the water connectivity of different RVEs at different hydration degrees is almost the same. This finding differs from the results reported by Zhang et al. [38], in whose study the connectivity of

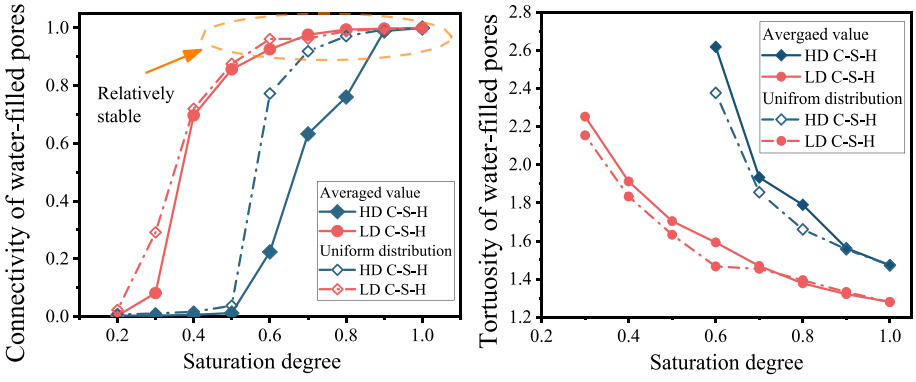

(a) Connectivity (b) Tortuosity

Fig. 14. Pore structure characteristics in unsaturated C-S-H gels.

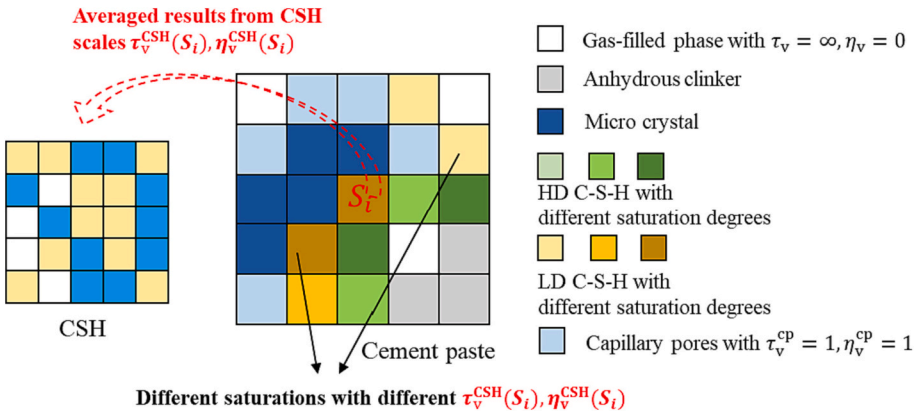

Fig. 15. Determination of pore structure characteristics at the cement paste level.

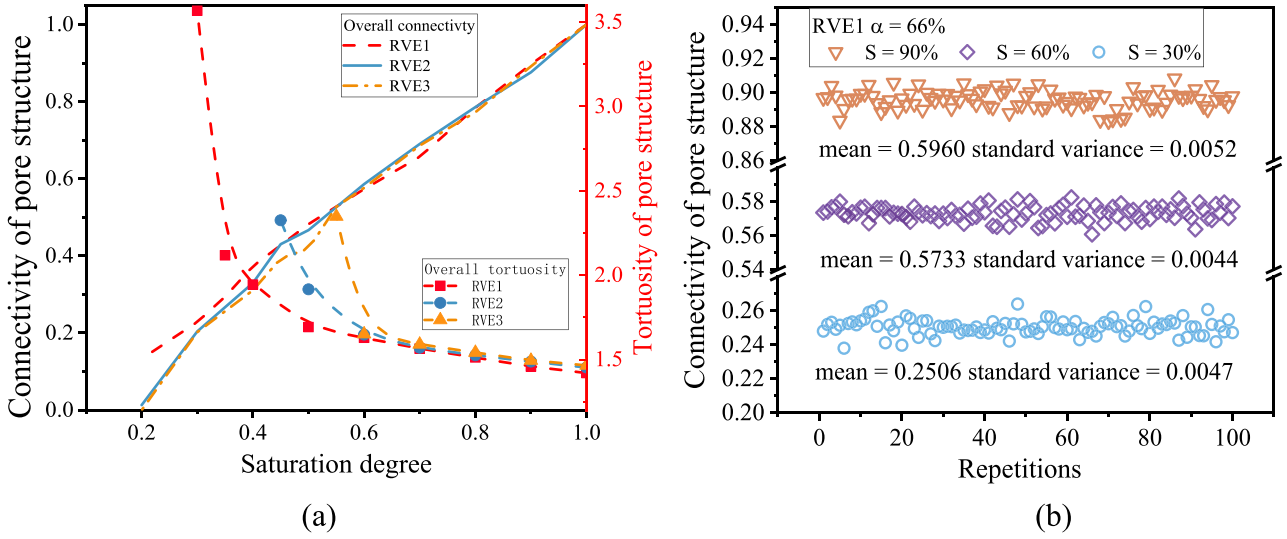

Fig. 16. Pore structure characteristics in unsaturated cement paste.
(a) Connectivity and tortuosity (b) Validation of stability.

pore structure drops significantly with the increased hydration degree as C-S-H level. This is mainly because their research does not consider the diffusivity of gel pores in C-S-H gels. Taking $\alpha = 82\%$ with $\varnothing_{cp} = 17.98\%$ as an example, as illustrated in Fig. 5(b), if only capillary pores are considered, the connected fraction of capillary pores is nearly 0. This means the cement paste is impermeable even if it is saturated. This is unrealistic. Thus, this finding also indicates the importance of considering the gel pores at the unsaturated stage.

The RVEs of C-S-H gels are applied with randomised cyclic drying-wetting processes. Section 5.1 has compared the differences between averaged values and results based on RVEs with uniformly distributed water. However, at the cement paste level, the water distributions of different slices are modelled as relatively homogeneous. Repeated simulation results are shown in Fig. 16(b) to discuss the stability of this method. Taking RVE1 as an example, 100 repetitions were simulated to model the uniform water distribution at saturation degrees 90 %, 60 %, and 30 %. Based on the listed mean and standard variance, the data indicates that relatively stable results can be obtained based on the RVEs with uniformly distributed water. Considering that the transport properties of unsaturated cement paste are highly related to their pore structure characteristics, such as water connectivity and water tortuosity, it is reasonable to estimate that such unsaturated RVEs can give relatively stable results in diffusivity prediction, and the prediction of chloride diffusivity will be discussed in the next section.

6. Prediction of chloride diffusivity at different levels

The simulated unsaturated RVEs of C-S-H gels and cement paste consist of different hydration products and clinkers, which own specific chloride diffusion coefficients at different saturations. By converting the voxel-based RVEs into a lattice diffusion network, the chloride diffusivity of unsaturated C-S-H gels and cement paste at a specific saturation degree (S) can be predicted. To achieve that, the lattice diffusive prediction model will be introduced and validated in this section.

6.1. Lattice diffusive prediction model

Fig. 17 illustrates the procedures to convert the generated RVEs of C-S-H gels and cement paste into the lattice diffusion networks (2D slice). To predict the chloride diffusion coefficient at a specific saturation degree, the following assumptions are addressed in the modelling: (1) Chloride ions can only diffuse within the continuous water-filled pores of voxels in the prediction, and diffusion occurs between the face-to-face voxel as pre-mentioned in Fig. 9(a); (2) C-S-H particles, anhydrous clinkers, micro crystals and voxels with saturation 0 % are converted into a solid-like node, which is considered impermeable; (3) No ionic flux is allowed to pass through the other four surfaces except for the inlet and the outlet.

For each voxel, it relates to a lattice node. The node presents a spe-

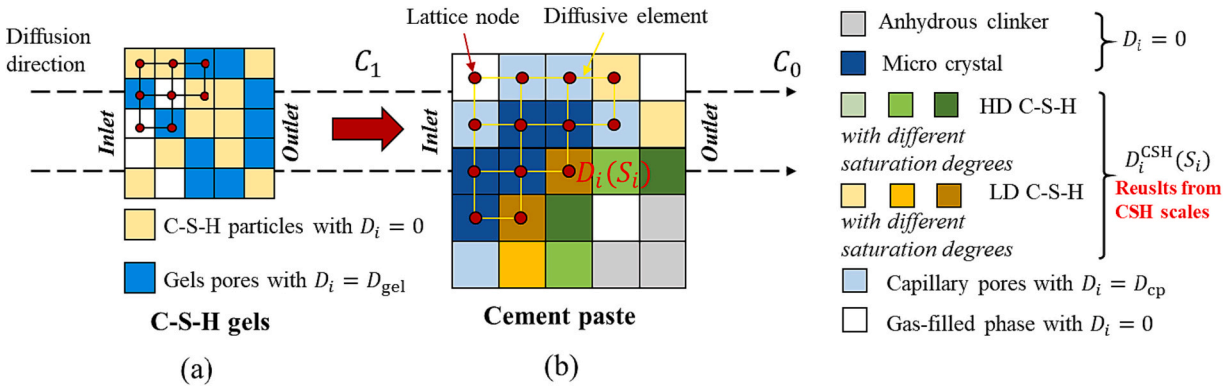

Fig. 17. Diffusion lattice networks (2D slice).
(a) C-S-H gels (b) Cement paste.

cific phase and links to a node diffusion coefficient D_i. For the diffusive element $i-j$ which connects node i and node j, the diffusion coefficient D_{i-j} is given as:

$$D_{i-j} = \frac{2}{\frac{1}{D_i} + \frac{1}{D_j}} \tag{8}$$

where D_i and D_j is the diffusion coefficient of lattice node i and j, respectively. In this study, each lattice node's chloride diffusion coefficient corresponds to its representative phase. Besides, it should be noted that either D_i or D_j is zero, D_{i-j} should be zero. As shown in Fig. 17(a, b), diffusivities of water-filled gel pores are defined as D_{gel} at the C-S-H level, and diffusivities of water-filled capillary pores are considered as D_{cp}. As reported by [88], the results obtained from molecular dynamics (MD) simulations on tobermorite and nuclear magnetic resonance (NMR) measures on cement pastes have evidenced that the diffusive transport in confined pores can be lower than in bulk water. Based on the electrical double layer (EDL) theory, a study by Nguyen and Amiri [89] conducted that a pore radius smaller than 2–3 nm will affect the diffusivities of chloride, while this effect can be neglected for larger pores. What's more, MD simulation in the capillary pores has been reported as $2 \times 10^{-9} m^2/s$, which is only slightly below the chloride diffusivity of bulk water ($2.03 \times 10^{-9} m^2/s$) [56,88]. Based on these results, it seems it is more appropriate to assume that the diffusion coefficient in water-filled capillary pores D_{cp} is close to that in bulk water D_{bulk}, and to consider the slow-down effect in gel pores. According to the inverse analysis done by Achour et al. [12], the chloride diffusivity in gel pores D_{gel} is defined as $0.0246 D_{bulk}$ in the proposed model. Similar to determining pore structure characteristics, chloride diffusivities of C-S-H voxels at the cement paste level with different saturation degrees are obtained through a multiscale computational homogenisation method, as shown in Fig. 17(b).

To investigate the intrinsic effect of pore structure characteristics on unsaturated cementitious materials, the steady-state diffusion process is considered in the present study, and the chloride binding effect is not taken into account, which is also adopted in [17,73]. In this situation, the diffusion process in cementitious materials is satisfied with Fick's first law. The flow along the element $i-j$ can be described as [73]:

$$q_{i-j} = -D_{i-j} \nabla c_{i-j} \tag{9}$$

where q_{i-j} is the flow density between node i and j, ∇c_{i-j} is the concentration gradient between the face-to-face lattices. During the modelling, q_{i-j} is positive for inflow and negative for outflow. It is known that the diffusion process converts from a non-steady-state to a steady state, and the chloride flux through the outlet surface will achieve a constant value when a steady state arrives. Thus, for each node at steady-state, the inlet flux equals outlet flux and does not change with time. As displayed in Fig. 18(a), at steady state, the concentration of the

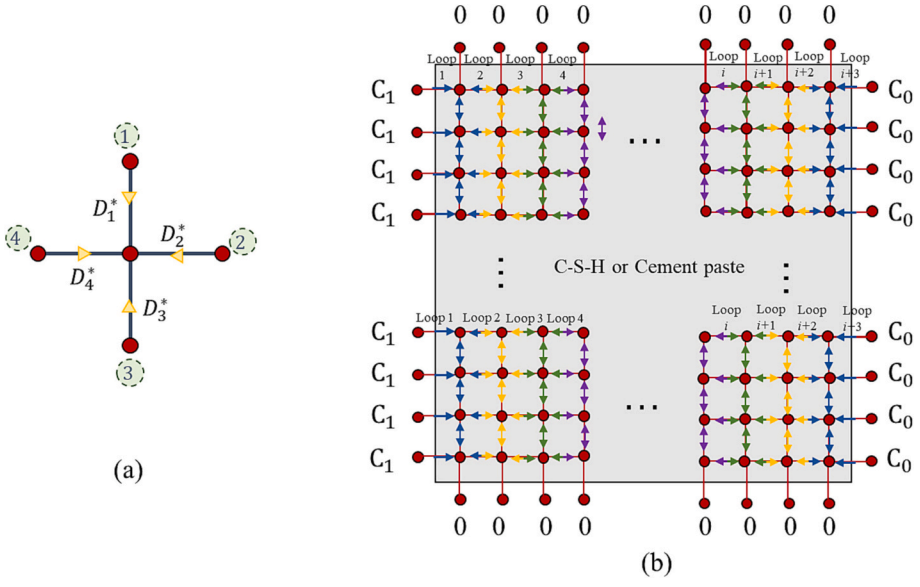

Fig. 18. A schematic diagram of (a) concentration calculation at each node (b) iterative process for steady-state chloride diffusion prediction.

node i can be calculated as:

$$D_1^*(C_1 - C_i) + D_2^*(C_2 - C_i) + D_3^*(C_2 - C_i) + D_4^*(C_2 - C_i) = 0 \quad (10)$$

$$C_i = \frac{D_1^* C_1 + D_2^* C_2 + D_3^* C_3 + D_4^* C_4}{D_1^* + D_2^* + D_3^* + D_4^*} \quad (11)$$

1, 2, 3 and 4 present four neighbouring nodes around the node i; D_1^*, D_2^*, D_3^* and D_4^* are the diffusivities between nodes 1 and i, nodes 2 and i, nodes 3 and i, nodes 4 and i, respectively as shown in Fig. 18(a). The steady-state can be achieved by iterating the concentrations until the outlet flux reach unchanged, as presented in Fig. 18(b). To initialize the iterative procedures, the initial chloride concentration of each node in the lattice model is set as zero, and the concentration of inlet and outlet are set as C_1 and C_0, which are 10 mol/m^3 and 0 mol/m^3 in present study, respectively. Conjugate gradient method (CGM) [73] is adopted in present study to accelerate the computation speed. After the steady-state is achieved, the modelled diffusion coefficient D (m^2/s) of C-S-H gels and cement paste at specific S, can be obtained by:

$$D(S) = \frac{Q}{A}\frac{L}{C_1 - C_0} \quad (12)$$

where Q is total flux through the outlet surface (mol/s), L is the length of sample (m), and A is the area of outlet surface (m^2). So, the relative chloride diffusion coefficient can be calculated as:

$$D_{rc}(S) = \frac{D(S)}{D(S = 100\%)} \quad (13)$$

Considering that the impermeable and gas-filled phases have no contribution to the diffusion process, it is efficient to identify and remove them from the iterative domain to reduce the memory demand and improve the computational efficiency.

6.2. Validation of predicted results with experimental data

6.2.1. C-S-H level

Fig. 19 displays the steady-state ionic concentration distribution in unsaturated C-S-H gels corresponding to those shown in Fig. 11. The tortuosity of water-filled pores in HD C-S-H at saturation degree 30 % is ∞. Hence the RVE of C-S-H at saturation degree 30 % becomes impermeable.

The averaged chloride diffusivities in unsaturated C-S-H gels against the water saturation degree is presented in Fig. 20. At saturated stage, the predicted results of chloride diffusivity in HD and LD C-S-H are found to be equal to $4.53 \times 10^{-4} D_{bulk}$ and $1.34 \times 10^{-3} D_{bulk}$ respectively. This result shows an acceptable agreement with the results reported by Achour et al. [12] ($D_{HDCSH} = 4.4 \times 10^{-4} D_{bulk}$, $D_{LDCSH} 1.6 \times 10^{-3} D_{bulk}$) and the results by Bary and Béjaoui [90] ($D_{HDCSH} = 3.7 \times 10^{-4} D_{bulk}$, $D_{LDCSH} = 1.5 \times 10^{-3} D_{bulk}$). It can be seen in Fig. 20 that the ionic diffusivities gradually decrease with the dropping of water saturation degree, which corresponds to the decreasing connectivity of water-filled pores as illustrated in Fig. 14. When the saturation degree reduces to 30 % in LD C-S-H and 60 % in HD C-S-H, the partially water-filled C-S-H gels are impermeable. Fig. 20 also indicates that finer pore structure owns a relatively lower ionic diffusivity at the same saturation degree.

6.2.2. Cement paste level

To verify the proposed lattice model at the cement paste level, herein, third-party tested relative chloride diffusion coefficients D_{rc} of

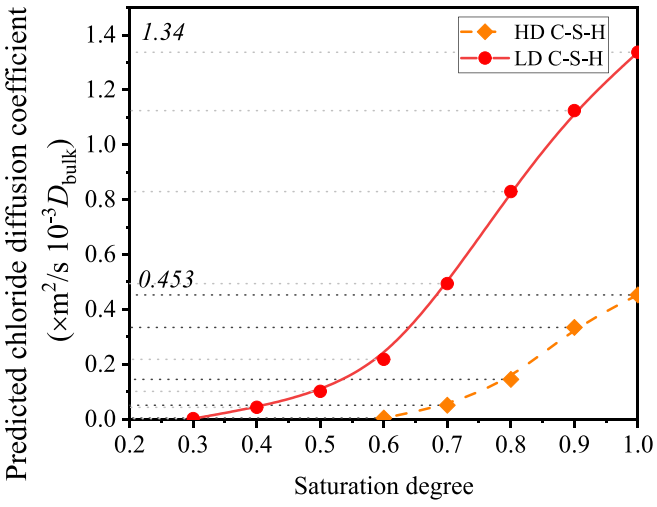

Fig. 20. Predicted chloride diffusivity of HD/LD C-S-H gels against different saturation degree.

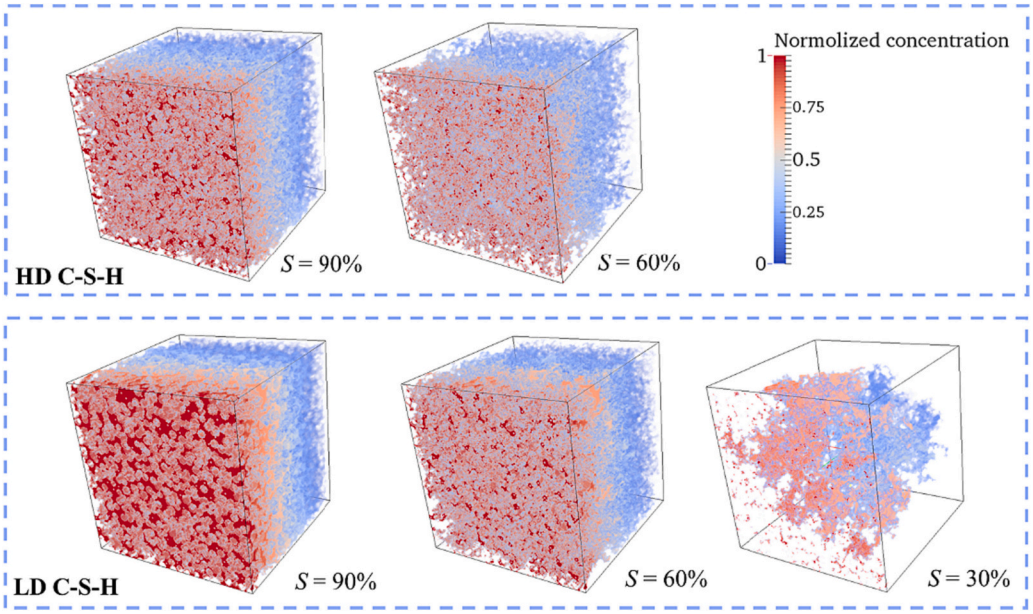

Fig. 19. Steady-state chloride concentration distribution of RVEs at C-S-H level.

cementitious materials with w/c 0.5 at different water saturation degrees are compared with the predicted relative chloride diffusion coefficients, which are obtained based on the uniform water distributed microstructure. The RVEs of cement paste used for relative chloride diffusion coefficient prediction are consistent with that discussed in Sections 3, 4 and 5. Detailed parameters of these three RVEs are listed in Table 1. The experimental results used to validate the proposed model are listed in Table 2.

Fig. 21 displays the steady-state chloride concentration distribution of different RVEs at saturation degrees 90 %, 60 %, and 30 % in cement paste. The chloride concentration distributions in the capillary pores were also isolated and demonstrated in Fig. 21. When the saturation degree is high, e.g., 90 %, it can be found that a large part of capillary pores plays a role in chloride diffusion. However, with the saturation degree decreasing, the main diffusion channels have been transformed from the capillary pores to partially water-filled C-S-H gels. The RVE with a higher hydration degree shows this trend more pronouncedly.

With the modelled results, the relative chloride diffusion coefficients ($D_{rc}(S)$) can be calculated. Fig. 22 shows the relative chloride diffusion coefficients of three RVEs against different water saturation degrees with a w/c ratio of 0.5. Obviously, the relative chloride diffusivity is highly related to the water saturation degrees. It can be observed that the increasing saturation degree can prompt chloride diffusion in cement paste. Increasing hydration degree can make the pore structure denser and reduce porosity, leading to a low diffusion coefficient at the same saturation degree. There is a significant decrease in diffusion coefficient when the water saturation degree reduces from 100 % to approximately 70 %, followed by a less sharp decline with the range 70 % to 40 %. When the saturation degree drops to approximately 40 %, the chloride diffusion coefficient approaches zero because no connected path is available. Fig. 22 also compares predicted and experimental results, showing a similar trend. It suggests that the relative chloride diffusion coefficient of cement paste can be predicted through the proposed lattice diffusion model. However, some specimens tested in experiments are mortars. Since mortar consists of cement paste and sand, the chloride diffusion coefficient of mortar can be adjusted by a parameter called f_s, which is related to the volume fraction of sand [46,94]. Assuming that sand is impermeable, the value of f_s will remain constant at different saturation degrees. Therefore, at an unsaturated state, the relative chloride diffusivity D_{rc} of the mortar can is equal to the relative diffusion coefficient of cement paste. Based on this point, the experimental results of mortar in Table 2 were used for model validation [38,39,66]. After model validation, the effect of pore structure characteristics and the water distribution caused by the water loading process on the chloride diffusivity of unsaturated cement paste will be further discussed in the next section.

7. Results and discussion

7.1. Effect of gel pores on chloride diffusivity at different hydration degrees

The gel pores in C-S-H gels play a critical role in chloride diffusivity in unsaturated cementitious materials. To further explore the relationship between the volume fraction of gel pores in pore structure and chloride diffusivity, RVEs at different hydration degrees with a saturation degree of 50 % were generated. Water contents at different slices are modelled as uniformly distributed, as illustrated in Section 4.2.

Table 1
The parameter of simulated samples.

Index	w/c	Days	Hydration degree	Capillary porosity
RVE 1	0.5	7	66 %	0.2477
RVE 2	0.5	14	82 %	0.1798
RVE 3	0.5	28	91 %	0.1387

Table 2
The third-party experimental results.

Authors	w/c	Binder type	Specimen	Curing ages
Guimarães et al. [91]	0.5	CEM II/A-L 32.5 R; CEM II/A-L 42.5 R	Mortar	28 days
Olsson et al. [92]	0.5	CEM I 42.5 N	Mortar	6 months
Olsson et al. [26]	0.53			3 months
Zhang et al. [55]	0.5	CEM I	Cement paste	1 year
Rajabipour [93]	0.5	ASTM Type I	Cement paste	3 months
Nielsen and Geiker [25]	0.5	Rapid Hardening Portland Cement	Mortar	~4.6 months

Fig. 23(a) displays that the predicted chloride diffusivity decreases with increasing hydration degrees, and there is a sharp decline within the range of 14 % to 39 % and keeps almost constant after 48 %. On the one hand, this is related to the denser pore structure caused by evolved hydration. On the other hand, this can be further explained based on the water proportion distributed in pore structures. Fig. 23(b) shows the water proportion distributed in gel and capillary pores at different hydration degrees. With the hydration degree increasing, the water distributed in capillary pores generally decreases. As highlighted by green and red columns (First four RVEs), at relatively lower hydration degrees, the water distributed in capillary pores is significantly higher than water distributed by gel pores, corresponding to the larger chloride diffusivity shown in Fig. 23(a) (red points). Since the hydration degree reaches 48 %, the main diffusion channels transform from the connected capillary pores to the serial connections of capillary pores entrapped by gel pores and finally to the partially saturated C-S-H network. A sharp decline appears because the chloride diffusivity in capillary pores is >1000 times higher than in gel pores [12].

Besides, Fig. 24 displays that the volume fraction of gel pores in the original pore structure grows steadily with the hydration evolved. Combined with the predicted relative chloride diffusion coefficients in Section 6, it can be found that there is a good match between the volume fraction of gel pores and the critical saturation degree at D_{rc}<10 %. Water tends to fill smaller pores, while gas prefers larger ones. Therefore, when the saturation degree is below the volume fraction of gel pores in the pore structure, the main diffusion channels are mainly the partially saturated C-S-H network with trapped capillary pores, which results in a constrict to chloride diffusion.

7.2. Effect of water distribution on chloride diffusivity considering drying-wetting processes

As briefly illustrated in Fig. 14, the averaged pore structure characteristics of C-S-H gels applied to randomised cyclic drying-wetting cycles differ from those determined based on RVEs with uniformly distributed water. Due to the complexity of the pore structure, different drying-wetting processes will influence the water distribution of the pore structure in hardened cement paste, resulting in a variance in chloride diffusivity even if the saturation degree remains constant. This section will model the water distribution applied to a single wetting or drying process and compare the predicted chloride diffusivity with the data obtained in Section 6 (with uniformly distributed water). It should be noted that the drying-wetting cycles are applied just to simulate water distribution instead of applying to the chloride diffusion process, which needs further investigation in the future.

RVE1 and RVE2 are selected as examples to present two conditions: better connectivity of capillary pores and Poor connectivity, as discussed in Fig. 5(b). Fig. 25 show the modelled water saturation at different slices during progressive wetting of these two RVEs. As displayed in Fig. 24, the pore structure of RVE1 is composed of 35 % gel pores, and RVE2 contains 48 % gel pores by volume. Since the water phase tends to

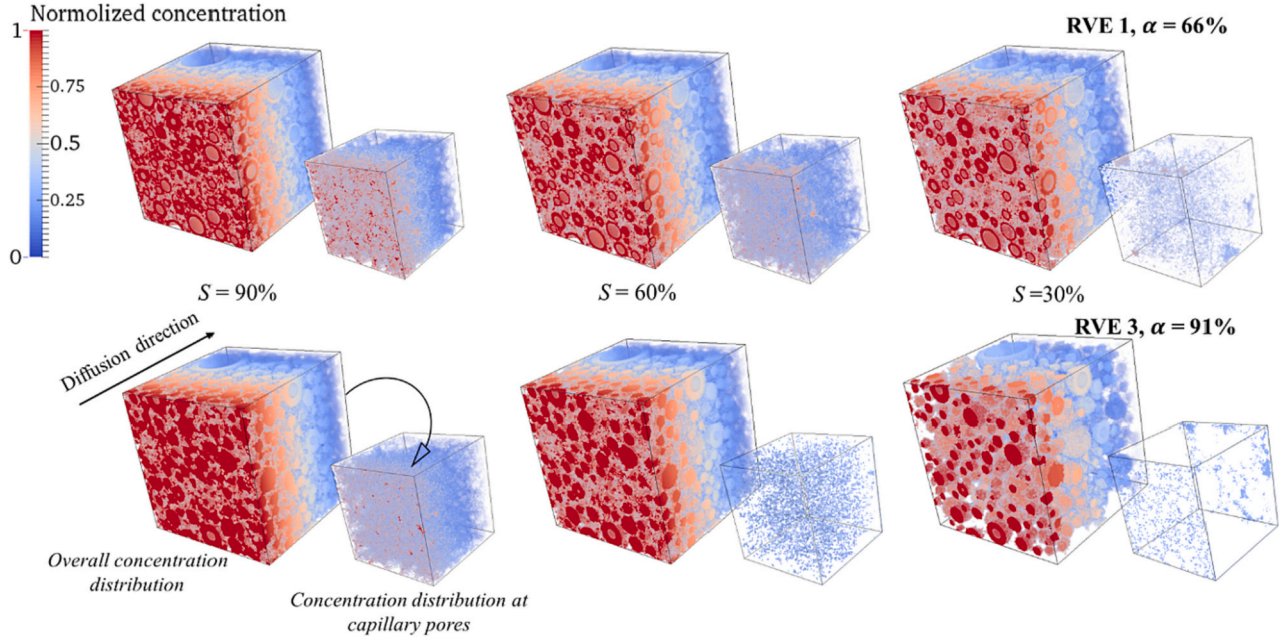

Fig. 21. Steady-state chloride concentration distribution of RVEs at cement paste level.

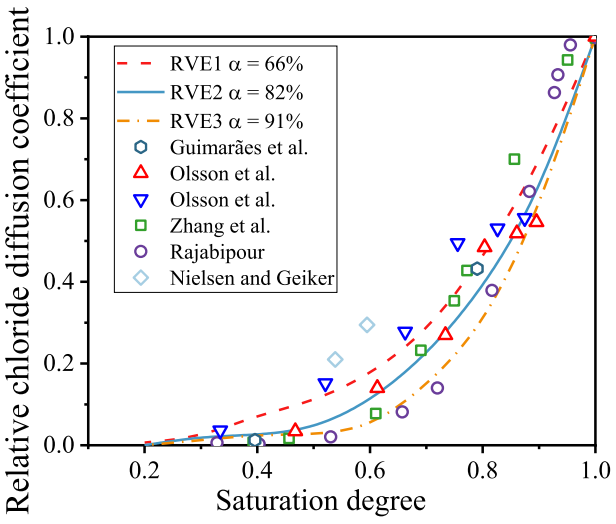

Fig. 22. Comparison of predicted and tested D_{rc} of unsaturated cement paste against different saturation degrees.

fill the small pores in porous media [64]. Thus, when the saturation degree is below 35 % in RVE1 and 48 % in RVE2, there is no water phase in capillary pores and gel pores become partially saturated. Beyond the fraction, the water will gradually fill the capillary pores from the surface, as indicated by the arrow in Fig. 25(a). The volume fraction of gel pores increases with the increasing hydration degree, as indicated by the arrow in Fig. 25(b).

Water saturations at different slices during progressive drying of RVE1 and RVE2 are shown in Fig. 26. During the drying process, the gas phase prefers to fill the larger pores. Considering the water trapping effect, the water drying process first occurs through the connected capillary pores. RVE1 comprises 65 % capillary pores in which 54 % is connected (illustrated in Section 3.1). Thus, in RVE1, the C-S-H gels remain saturated until the saturation degree below $1 - 65\% \times 50\% = 64.9\%$ as highlighted in Fig. 26(a). Due to the relatively better connectivity of capillary pores, there are more or less C-S-H gels at each slice in contact with the dried capillary pores and can begin to dry when continuously decreasing saturations. So, all slices could dry more uniformly, and no obvious dry-wet interface exists. On the contrary, the connectivity of capillary pores in RVE2 is poor, most capillary pores are trapped by C-S-H gels. Therefore, there is an obvious dry-wet interface, as shown in Fig. 26(b). Only the former slice has lost its water, and the latter can then begin to dry. In this condition, the slice saturation away from the surface is much larger than the slice saturation near the surface.

Fig. 27 shows the saturation degree of capillary pores during progressive wetting and drying in RVE 1 and RVE2. The gap between the two lines indicates the fraction of trapped water in capillary pores. The fraction of trapped water in RVE2 is higher than in RVE1 due to the poor connectivity of capillary pores. Considering the relatively coarser pore structure in RVE1, higher saturation of capillary pores at the same saturation degree can promote chloride diffusion. As shown in Fig. 28 (a), the tortuosity of transport channels during a single drying process is relatively lower than that during progressive wetting. On the contrary, the almost dried surface in RVE2 leads to a significant rise of tortuosity at a lower saturation degree, as shown in Fig. 28(b). Considering that the uniformly distributed water is applied with a cyclic drying-wetting process, the tortuosity also lies between the single wetting and drying process. The predicted chloride diffusivity shows consistent trends with predicted tortuosity, as shown by the right y-axis in Fig. 28. In conclusion, when the connectivity of capillary pores is comparatively good, higher saturation of capillary pores can lead to higher chloride diffusivity, with $D_W < D_U < D_D$. Otherwise, the drying process of dense pore structure will cause the surface to dry out quickly, leading to the decrease of chloride diffusivity, with $D_W > D_U > D_D$.

Predicted chloride diffusivity during progressive wetting D_W; during progressive drying D_D; with uniformly distributed water D_U.

7.3. Relative diffusion coefficient based on multiple-typed pore structure characteristics

In unsaturated hardened cement paste, not only saturation degree but also pore structure characteristics can influence the chloride diffusion properties. In this Section, a prediction equation for D_{rc} will be proposed based on multiple-typed pore structure characteristics. The comparisons of existing and novel models on the predicted D_{rc}-value are also further analysed.

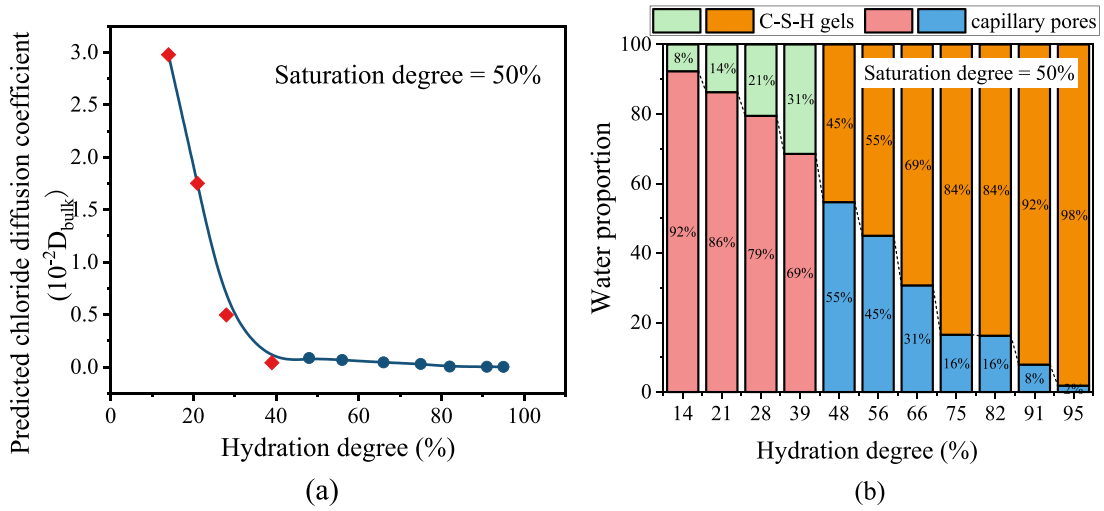

Fig. 23. Effect on hydration degrees on(a) Predicted chloride diffusivity, (b) Water proportion.

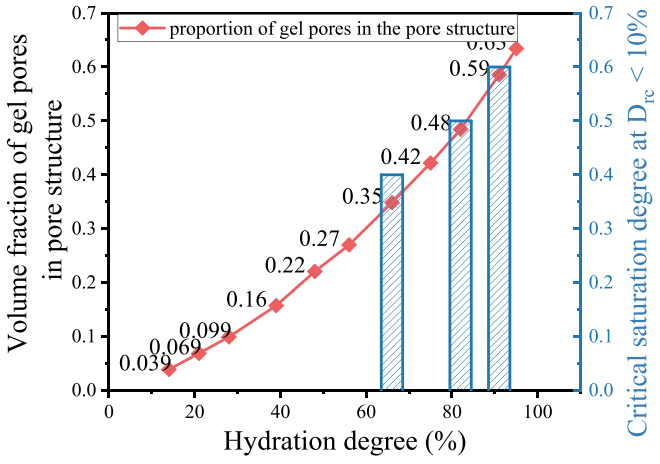

Fig. 24. Relationship between volume fraction of gel pores and critical saturation degree.

7.3.1. An analytical equation for relative diffusion coefficient prediction

Generally, the diffusivities of cementitious materials decrease with the increasing water tortuosity because more diffusion distance is needed to pass, and with the drop of water connectivity due to less connected channels are accessible. As mentioned in the introduction, some previous work tried to clarify the dependence of the relative diffusion coefficient on moisture content or saturation degree. However, these equations cannot fully account for the dependence of ionic diffusion on pore structure.

It was well known that the relationship between diffusion coefficient and pore tortuosity can be given by effective media theory (Eq. (14)) [33,95].

$$D_{\text{Paste}} = \frac{\delta_{\text{paste}}}{\tau^2_{\text{Paste}}} D_{\text{bulk}} \tag{14}$$

where, D_{Paste} is the apparent chloride diffusion coefficient of cement paste, δ_{paste} is the constrictivity of pore structure, thus the D_{rc}-value at different saturation degree (S), should be described as:

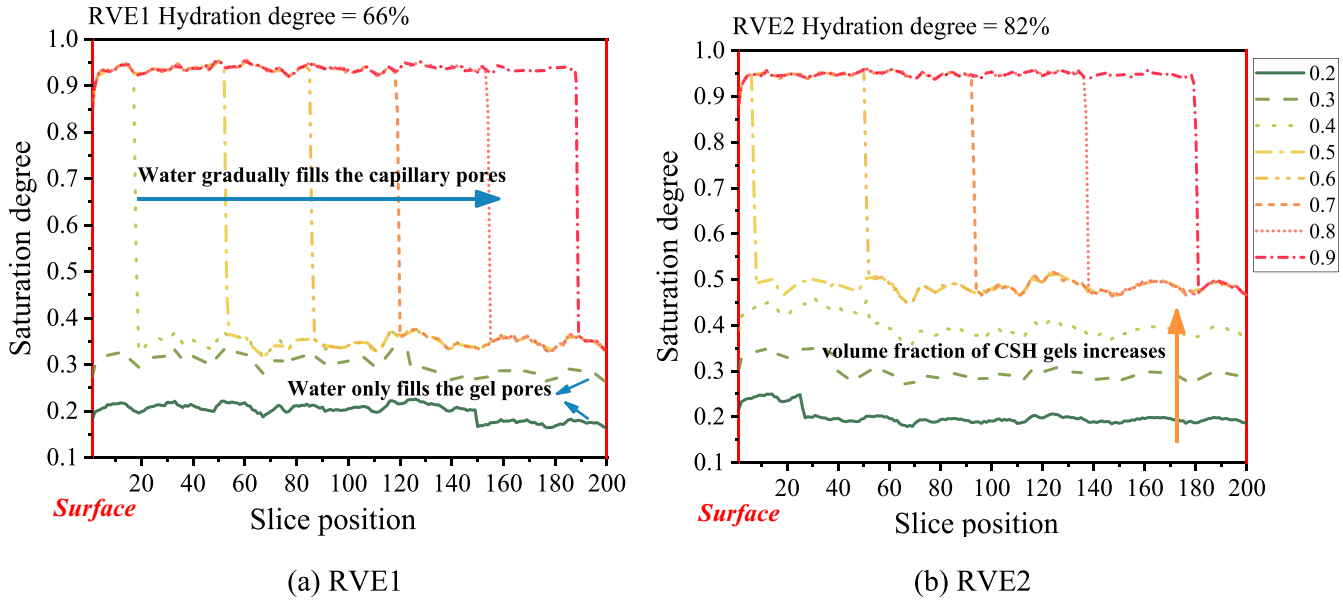

Fig. 25. Saturation degrees at different slices during the progressive wetting process.

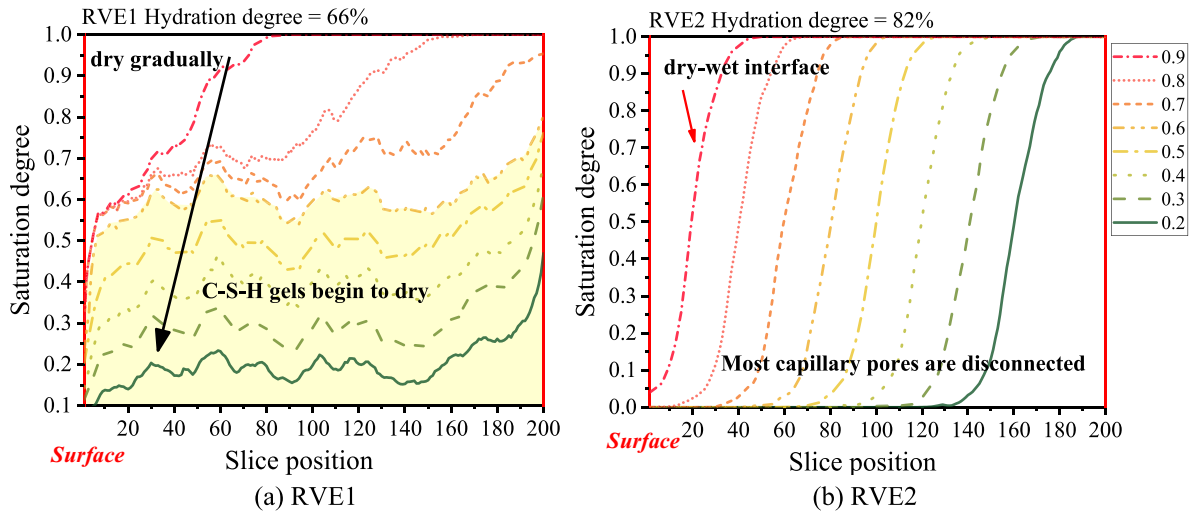

Fig. 26. Saturation degrees at different slices during progressive drying process.

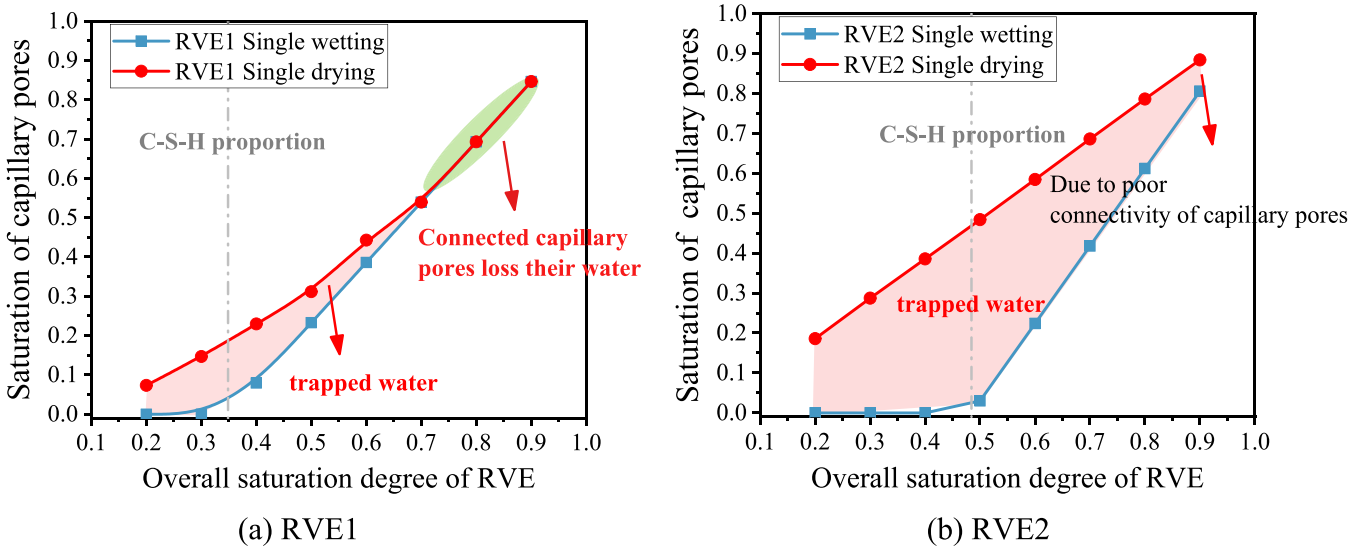

Fig. 27. Saturation degrees of capillary pores considering different drying-wetting processes.

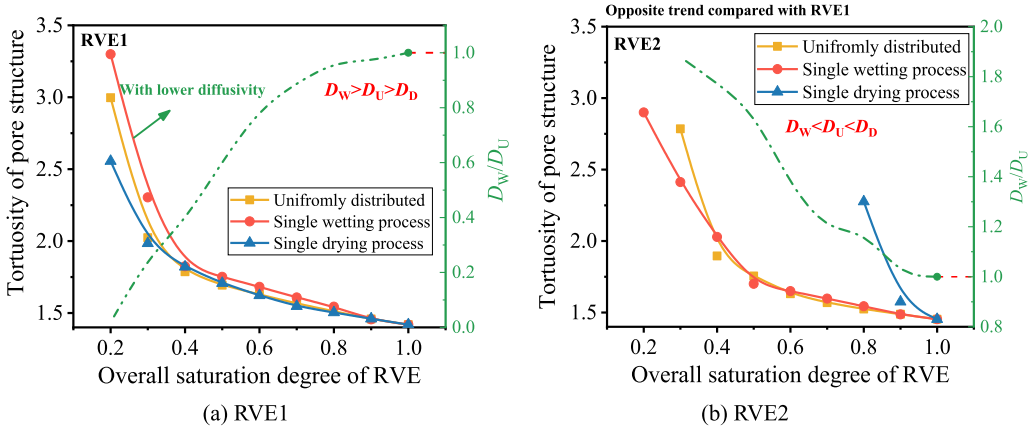

Fig. 28. Tortuosity of hardened cement paste considering different drying-wetting processes.

$$D_{rc}(S) = \frac{\delta^{rc}_{Paste}(S)}{\tau^{rc}_{Paste}(S)^2} \quad (15)$$

where $\delta^{rc}_{Paste}(S) = \frac{\delta_{paste}(S)}{\delta_{paste}(S=100\%)}$ and $\tau^{rc}_{Paste}(S) = \frac{\tau_{Paste}(S)}{\tau_{Paste}(S=100\%)}$. Besides, as derived in Zhang's work [55], D_{rc} can be expressed as the function of saturation degree (S) and connectivity (η_{Paste}). Inspired by these two equations and based on the modelled results, a new prediction equation for D_{rc} is inspired with the consideration of saturation degree (S), water connectivity ($\eta_{Paste}(S)$) and relative water tortuosity ($\tau^{rc}_{Paste}(S)$) as:

$$D_{rc}(S) = \frac{S^{\beta}\eta_{Paste}(S)}{\tau^{rc}_{Paste}(S)^2} \quad (16)$$

η_{Paste} and τ^{rc}_{Paste} can be extracted based on the redistributed RVEs as illustrated before, β is a fitting parameter. The pore system characteristics of three RVEs and fitted relative chloride diffusion coefficient by Eq. (16) are listed in Table 3.

Since the D_{rc} obtained from the lattice diffusive model through Eq. (13) has been experimentally validated as shown in Fig. 22, so, the D_{rc} (Eq. (13)) is treated as approximate experimental data in this section, and shown by the blue columns in Table 3. The green columns show the fitted D_{rc} by Eq. (16). Fig. 29 shows the comparison of modelled and fitted values. Based on root-mean-square error (RMSE), it can be seen that Eq. (16) can achieve good fitting accuracy. This concise equation can characterise the effect of pore structure on the relative chloride diffusion coefficient, including the gas blocking and tortuous diffusive channels.

7.3.2. Comparison between existing and proposed models

The relationship between saturation degree (S) and relative chloride diffusion coefficient (D_{rc}) can be predicted by existing empirical equations (Eqs. (2) and (3)) and novel proposed prediction equations (Eq. (16)). The RMSE obtained based on different equations or parameters are shown in Fig. 30. Compared with quadratic polynomial equation (Eq. (3)), the novel proposed model always indicates a better fitting accuracy. If defining the λ as 6 [28] or 4.5 [26] in the power equation, it can be seen that the RMSE shows a significant fluctuation in different RVEs. If better accuracy is desired, λ should be 3.472, 4.838 and 5.480 for three RVEs, respectively. However, accuracy aside, neither the quadratic polynomial nor the power equation can fully account for the dependency of ionic diffusion on the pore structure and the water distribution at an unsaturated state.

In the present study, original capillary pores are redistributed to

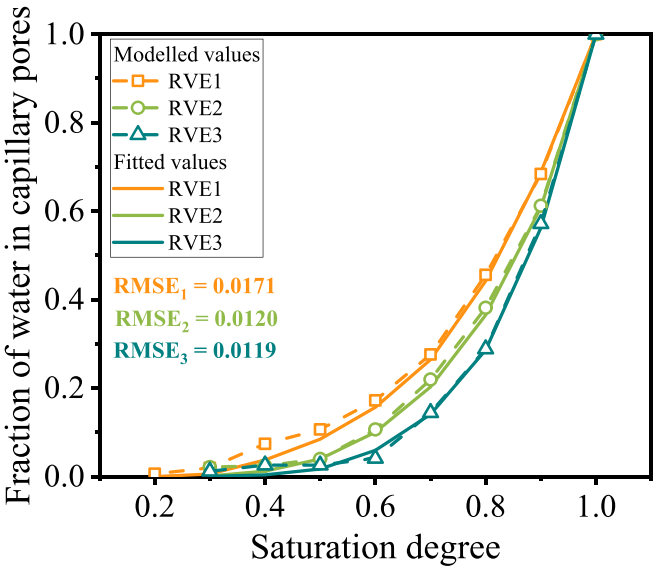

Fig. 29. Comparison of modelled and fitted D_{rc}-value.

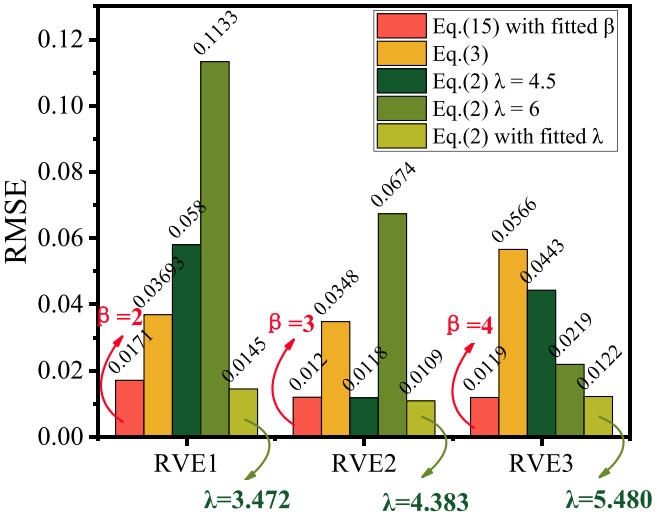

Fig. 30. Calculated RMSEs based on different equations or parameters.

Table 3
The pore system characteristics and their relationship between relative diffusion coefficient.

Specimen	RVE 1				RVE 2				RVE 3			
S	Pore structure characteristics and relative diffusion coefficient (modelled and fitted)											
	D_{rc} Eq. (13)	η_{Paste}	τ^{rc}_{Paste}	D_{rc} Eq. (16)	D_{rc} Eq. (13)	η_{Paste}	τ^{rc}_{Paste}	D_{rc} Eq. (16)	D_{rc} Eq. (13)	η_{Paste}	τ^{rc}_{Paste}	D_{rc} Eq. (16)
β	$\beta = 2$				$\beta = 3$				$\beta = 4$			
1	1.0000	1.00	1.00	1.0000	1.0000	1.00	1.00	1.0000	1.0000	1.00	1.00	1.0000
0.9	0.6841	0.90	1.03	0.6882	0.6124	0.88	1.02	0.6089	0.5719	0.89	1.02	0.5627
0.8	0.4561	0.78	1.07	0.4422	0.3818	0.79	1.05	0.3654	0.2888	0.77	1.05	0.2864
0.7	0.2762	0.66	1.10	0.2645	0.2196	0.69	1.08	0.2030	0.1447	0.69	1.08	0.1411
0.6	0.1723	0.57	1.15	0.1568	0.1067	0.59	1.12	0.1004	0.0413	0.58	1.12	0.0594
0.5	0.1066	0.48	1.19	0.0847	0.0398	0.47	1.21	0.0400	0.0261	0.42	1.23	0.0174
0.4	0.0742	0.37	1.26	0.0377	0.0247	0.33	1.30	0.0124	0.0259	0.31	1.41	0.0040
0.3	0.0197	0.23	1.43	0.0059	0.0214	0.20	1.92	0.0015	0.0123	0.23	2.04	0.0004
0.2	0.0065	0.13	2.11	0.0000								

Note: D_X means that the data is obtained through Eq. (X).
Blue columns: Modelled relative diffusivity by Eq. (13) Green columns: Fitted relative diffusivity by Eq. (16)

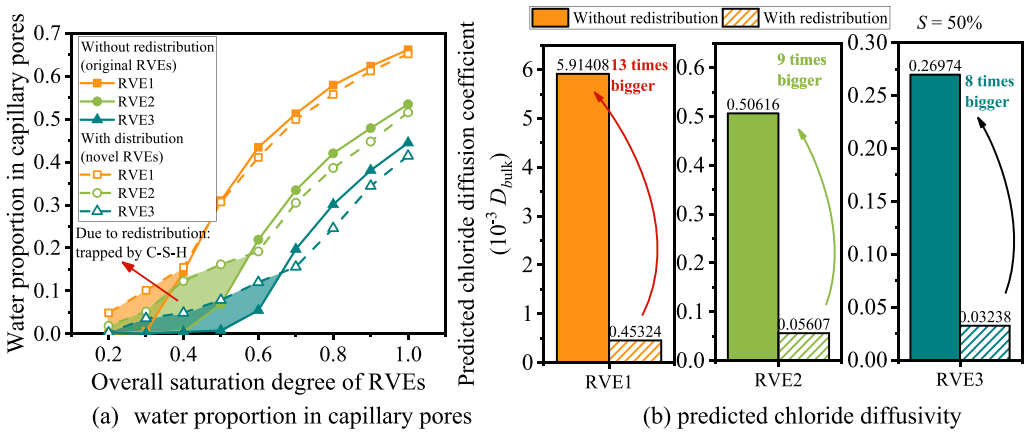

Fig. 31. Comparison between original RVEs and novel RVEs.

better represent the natural connectivity of capillary pores in hardened cement paste. By uniformly distributing the water at different slices in original and novel RVEs, Fig. 31(a) shows the proportion of water distributed in capillary pores. At higher saturation, the water content distributed in capillary pores in novel RVEs is lower than in original RVEs. However, at lower saturation, the fraction of water in capillary pores in novel RVEs is much higher due to the trapping of C-S-H gels. Fig. 31(b) shows the predicted chloride diffusivity at a saturation of 50 % based on the RVEs with or without redistribution of capillary pores. By modelling the steady-state diffusion, it can be seen that the predicted diffusivity based on the RVEs without redistribution can be nearly 8 to 10 times larger than that with redistribution. This is due to the higher connectivity of capillary pores in the original RVEs. A review by Patel [41] also reported that chloride diffusivity prediction based on spheres-based hydration models can overestimate experimental data by up to a factor of ten. But interestingly, it is also reported the relative diffusion coefficient at different saturation degree can be predicted in good accuracy by using undistributed microstructures and without the consideration of gel pores [19,38,73]. While disregarding the presence of C-S-H gels will underestimate the diffusivity, the overestimation caused by non-redistributed capillary pores may counteract the underestimation. This may be why these model shows relatively reasonable results in predicting relative chloride diffusivity at an unsaturated state. Based on the above comparison with the existing equations and traditional sphere-based model, it can be concluded that the novel proposed model can better demonstrate the actual microstructure of hardened cement paste and can predict the ionic diffusivity more accurately by taking into account the characteristics of unsaturated pore structure.

8. Conclusion

A numerical model for predicting the relative chloride diffusion coefficient in unsaturated cementitious materials is proposed in this paper. Based on the RVEs generated by μic, the capillary pores are redistributed to better represent the natural microstructure of hardened cement paste. The water distributions at unsaturated pore structures are modelled by applying cyclic drying-wetting loading processes, and the presence of gel pores in C-S-H gels is also considered. By transforming the voxel-based network into a diffusive network, chloride diffusivity is predicted based on the novel redistributed model. The predicted diffusion coefficient as a function of water saturation degree and pore structure characteristics agrees with experimental results obtained from the literature. Based on the present model, the following conclusions can be drawn:

(1) As the decreasing of saturation degree, the main transport channels for chloride diffusion will transform from the connected capillary pores to the serial connections of capillary pores entrapped by gel pores and finally to the partially saturated C-S-H network. Thus, the volume fraction of gel pores in pore structure can be an efficient indicator to estimate the critical saturation degree at $D_{rc} < 10\%$.

(2) Different drying-wetting processes applied to cement paste will influence the water distribution in unsaturated pore structure, further affecting the pore structure characteristics and chloride diffusivity. The saturation of capillary pores during the progressive drying process is higher than during the progressive wetting process due to trapping by gel pores in C-S-H gels.

(3) When the connectivity of capillary pores is comparatively good, higher saturation of capillary pores can lead to the higher chloride diffusivity, with $D_W < D_U < D_D$. If the connectivity of capillary pores is poor, the drying process of pore structure will cause the areas near the surface to dry out quickly, leading to the decrease of chloride diffusivity, with $D_W > D_U > D_D$.

(4) The ionic diffusion coefficient is strongly influenced by the water saturation degree and pore structure characteristics. The diffusion coefficient decreases significantly when the saturation degree drops from 100 % to 70 % approximately, and the declining trend becomes slow between 70 % and 40 %.

(5) A new D_{rc}—S relationship is expressed as an analytical equation with the consideration of multiple kinds of pore structure characteristics. Compared with existing empirical equations and traditional sphere-based models, the calculated RMSE indicates that the novel proposed model can better demonstrate the microstructure of hardened cement paste and predict the ionic diffusivity more accurately. This phenomenon proves the idea again that the multiple kinds of pore structure characteristics should be considered when predicting D_{rc}-value, and can overcome the inaccuracy of previous models based on single saturation degree or relative humidity.

CRediT authorship contribution statement

Liang-yu Tong: Conceptualization, Methodology, Data curation, Software, Visualization, Validation, Writing – original draft. **Qing Xiang Xiong:** Conceptualization, Formal analysis, Validation, Writing – review & editing. **Zhidong Zhang:** Methodology, Software, Visualization, Writing – review & editing. **Xiangsheng Chen:** Conceptualization, Supervision, Writing – review & editing. **Guang Ye:** Formal analysis, Writing – review & editing, Supervision. **Qing-feng Liu:** Writing – review & editing, Conceptualization, Methodology, Supervision, Project administration, Funding acquisition.

Declaration of competing interest

We declare that we have no financial or personal relationships with other people or organizations that can inappropriately influence our work. There is no professional or other personal interest of any nature or kind in any product, service and/or company that could be construed as influencing the position presented in, or the review of, the manuscript entitled "A novel lattice model to predict chloride diffusion coefficient of unsaturated cementitious materials based on multiple-typed pore structure characteristics".

Data availability

The data that has been used is confidential.

Acknowledgements

This work was funded by the National Natural Science Foundation of China (52222805, 51978396), the Natural Science Foundation of Shanghai, China (22ZR1431400), and the Oceanic Interdisciplinary Program of Shanghai Jiao Tong University, China (SL2021MS016).

Appendix A. Detailed pore structure characteristics at the C-S-H level

Table A1
Calculated connectivity of water-filled pores in HD C-S-H gels.

$\eta_{CSH}^{HD}(S)$	RVE1	RVE2	RVE3	RVE4	RVE5	RVE6	RVE7	RVE8	RVE9	RVE10
100 %	1	1	1	1	1	1	1	1	1	1
90 %	0.9942	0.9863	0.9947	0.9854	0.9879	0.9964	0.9616	0.9927	0.9879	0.9854
80 %	0.9648	0.9075	0.9675	0.0116	0.9642	0.9691	0.9693	0.9642	0.9657	0.0017
70 %	0.9241	0.0017	0.9185	0.0061	0.0017	0.9195	0.8515	0.9238	0.9317	0.0142
60 %	0.7475	0.0099	0.0018	0.0122	0.0052	0.0037	0.0006	0.7733	0.7724	0.0015
50 %	0.0022	0.0195	0.0061	0.0207	0.0038	0.0071	0.0017	0.0027	0.0525	0.0232
40 %	0.0077	0.0086	0.0051	0.0075	0.0058	0.0046	0.0052	0.0128	0.0113	0.0052
30 %	0.0023	0.0011	0.0010	0.0020	0.0066	0.0074	0.0032	0.0044	0.0003	0.0072
20 %	0.0036	0.0000	0.0038	0.0023	0.0045	0.0010	0.0029	0.0057	0.0000	0.0057

$\eta_{CSH}^{HD}(S)$	RVE11	RVE12	RVE13	RVE14	RVE15	RVE16	RVE17	RVE18	RVE19	RVE20
100 %	1	1	1	1	1	1	1	1	1	1
90 %	0.9980	0.9921	0.9966	0.9922	0.9839	0.9949	0.9863	0.9928	0.9872	0.9976
80 %	0.0005	0.9307	0.0020	0.9483	0.9637	0.9432	0.9515	0.8729	0.9577	0.9627
70 %	0.8610	0.9114	0.8589	0.9049	0.9143	0.0035	0.8961	0.9036	0.9154	0.0025
60 %	0.0175	0.0213	0.1187	0.6727	0.6053	0.6990	0.0018	0.0011	0.0032	0.0201
50 %	0.0454	0.0000	0.0061	0.0057	0.0175	0.0008	0.0153	0.0018	0.0031	0.0128
40 %	0.0002	0.0062	0.0006	0.0015	0.0116	0.0084	0.0008	0.0117	0.0095	0.0021
30 %	0.0000	0.0027	0.0061	0.0070	0.0000	0.0027	0.0059	0.0013	0.0074	0.0052
20 %	0.0016	0.0026	0.0056	0.0029	0.0038	0.0042	0.0054	0.0015	0.0024	0.0050

Table A2
Calculated connectivity of water-filled pores in LD C-S-H gels.

$\eta_{CSH}^{LD}(S)$	RVE1	RVE2	RVE3	RVE4	RVE5	RVE6	RVE7	RVE8	RVE9	RVE10
100 %	1	1	1	1	1	1	1	1	1	1
90 %	0.9985	0.9980	0.9981	0.9979	0.9986	0.9981	0.9980	0.9980	0.9981	0.9968
80 %	0.9965	0.9965	0.9925	0.9918	0.9967	0.9946	0.9966	0.9966	0.9935	0.9956
70 %	0.9862	0.9860	0.9809	0.9873	0.9865	0.9451	0.9853	0.9853	0.9675	0.9416
60 %	0.9428	0.9268	0.9282	0.9290	0.9337	0.9333	0.9211	0.9247	0.9270	0.9161
50 %	0.8569	0.8547	0.8466	0.8530	0.8684	0.8587	0.8569	0.8573	0.8589	0.8599
40 %	0.6656	0.7818	0.6647	0.6356	0.6805	0.6277	0.7580	0.7782	0.7589	0.6417
30 %	0.0082	0.0000	0.0126	0.0012	0.0039	0.0007	0.0160	0.0093	0.0154	0.0124
20 %	0.0041	0.0014	0.0022	0.0031	0.0036	0.0028	0.0006	0.0059	0.0039	0.0058

$\eta_{CSH}^{LD}(S)$	RVE11	RVE12	RVE13	RVE14	RVE15	RVE16	RVE17	RVE18	RVE19	RVE20
100 %	1	1	1	1	1	1	1	1	1	1
90 %	0.9901	0.9980	0.9981	0.9979	0.9980	0.9981	0.9974	0.9978	0.9986	0.9980
80 %	0.9964	0.9966	0.9960	0.9843	0.9966	0.9967	0.9958	0.9964	0.9879	0.9966
70 %	0.9572	0.9851	0.9677	0.9876	0.9867	0.9693	0.9866	0.9849	0.9751	0.9853
60 %	0.9387	0.9217	0.9301	0.9150	0.9431	0.9205	0.9177	0.9210	0.9216	0.9131
50 %	0.8469	0.8750	0.8495	0.8596	0.8525	0.8667	0.8554	0.8534	0.8506	0.8549
40 %	0.7697	0.7576	0.6518	0.7613	0.6910	0.7477	0.6822	0.6695	0.5946	0.6294
30 %	0.1909	0.3625	0.0085	0.0031	0.3891	0.0197	0.0160	0.0006	0.0043	0.5571
20 %	0.0003	0.0016	0.0018	0.0047	0.0032	0.0039	0.0006	0.0035	0.0066	0.0055

Table A3
Calculated tortuosity of water-filled pores in HD C-S-H gels.

$\tau_{CSH}^{HD}(S)$	RVE1	RVE2	RVE3	RVE4	RVE5	RVE6	RVE7	RVE8	RVE9	RVE10
100 %	1.4792	1.4719	1.4749	1.4697	1.4795	1.4841	1.4762	1.4756	1.4756	1.4692
90 %	1.5530	1.5612	1.5575	1.5770	1.5728	1.5559	1.6609	1.5528	1.5623	1.5752
80 %	1.6804	1.9690	1.6769	Inf	1.6798	1.6790	1.6625	1.6707	1.6648	Inf
70 %	1.8805	Inf	1.8896	Inf	Inf	1.8646	2.1478	1.8678	1.8354	Inf
60 %	2.4338	Inf	Inf	Inf	Inf	Inf	Inf	2.4018	2.3856	Inf
50 %	Inf	Inf	Inf	Inf	Inf	Inf	Inf	Inf	Inf	Inf
40 %	Inf	Inf	Inf	Inf	Inf	Inf	Inf	Inf	Inf	Inf
30 %	Inf	Inf	Inf	Inf	Inf	Inf	Inf	Inf	Inf	Inf
20 %	Inf	Inf	Inf	Inf	Inf	Inf	Inf	Inf	Inf	Inf

$\tau_{CSH}^{HD}(S)$	RVE11	RVE12	RVE13	RVE14	RVE15	RVE16	RVE17	RVE18	RVE19	RVE20
100 %	1.4812	1.4661	1.4661	1.4827	1.4619	1.4664	1.4664	1.4676	1.4769	1.4657
90 %	1.5379	1.5525	1.5357	1.5699	1.5690	1.5482	1.5607	1.5534	1.5607	1.5409
80 %	Inf	1.7839	Inf	1.7394	1.6691	1.7776	1.7536	2.8421	1.7095	1.6787
70 %	2.1044	1.8541	2.0480	1.8774	1.8841	Inf	1.9819	1.9265	1.9082	Inf
60 %	Inf	Inf	Inf	2.5190	3.4627	2.5060	Inf	Inf	Inf	Inf
50 %	Inf	Inf	Inf	Inf	Inf	Inf	Inf	Inf	Inf	Inf
40 %	Inf	Inf	Inf	Inf	Inf	Inf	Inf	Inf	Inf	Inf
30 %	Inf	Inf	Inf	Inf	Inf	Inf	Inf	Inf	Inf	Inf
20 %	Inf	Inf	Inf	Inf	Inf	Inf	Inf	Inf	Inf	Inf

Table A4
Calculated tortuosity of water-filled pores in LD C-S-H gels.

$\tau_{CSH}^{LD}(S)$	RVE1	RVE2	RVE3	RVE4	RVE5	RVE6	RVE7	RVE8	RVE9	RVE10
100 %	1.2798	1.2770	1.2828	1.2852	1.2792	1.2816	1.2790	1.2767	1.2798	1.2806
90 %	1.3207	1.3227	1.3164	1.3193	1.3222	1.3150	1.3197	1.3114	1.3192	1.3402
80 %	1.3702	1.3749	1.3889	1.3861	1.3586	1.3840	1.3736	1.3650	1.3926	1.3694
70 %	1.4662	1.4659	1.4681	1.4655	1.4675	1.4821	1.4684	1.4605	1.4751	1.4829
60 %	1.5989	1.5988	1.6031	1.6166	1.5559	1.5889	1.6007	1.5861	1.6097	1.5832
50 %	1.6849	1.6881	1.7384	1.7546	1.6882	1.7039	1.6750	1.6799	1.7258	1.6670
40 %	1.8695	1.8678	1.8594	1.9787	2.0261	1.9396	2.0471	1.8192	1.8660	1.8220
30 %	Inf	Inf	Inf	Inf	Inf	Inf	Inf	Inf	Inf	Inf
20 %	Inf	Inf	Inf	Inf	Inf	Inf	Inf	Inf	Inf	Inf

$\tau_{CSH}^{LD}(S)$	RVE11	RVE12	RVE13	RVE14	RVE15	RVE16	RVE17	RVE18	RVE19	RVE20
100 %	1.2867	1.2785	1.2760	1.2850	1.2785	1.2779	1.2752	1.2813	1.2845	1.2831
90 %	1.3477	1.3196	1.3131	1.3192	1.3183	1.3136	1.3220	1.3164	1.3283	1.3177
80 %	1.3764	1.3752	1.3780	1.4026	1.3710	1.3674	1.3739	1.3742	1.4043	1.3745
70 %	1.4603	1.4647	1.4713	1.4702	1.4676	1.4680	1.4684	1.4717	1.4723	1.4645
60 %	1.6107	1.6086	1.6085	1.5734	1.5975	1.5755	1.5878	1.5893	1.6101	1.5468
50 %	1.7566	1.6641	1.7145	1.6548	1.7023	1.6857	1.6758	1.6753	1.7851	1.7564
40 %	1.8834	1.8595	1.8006	2.0340	1.8069	2.0309	1.8342	1.8032	2.1364	1.9586
30 %	Inf	2.3446	Inf	Inf	2.3457	Inf	Inf	Inf	Inf	2.0663
20 %	Inf	Inf	Inf	Inf	Inf	Inf	Inf	Inf	Inf	Inf

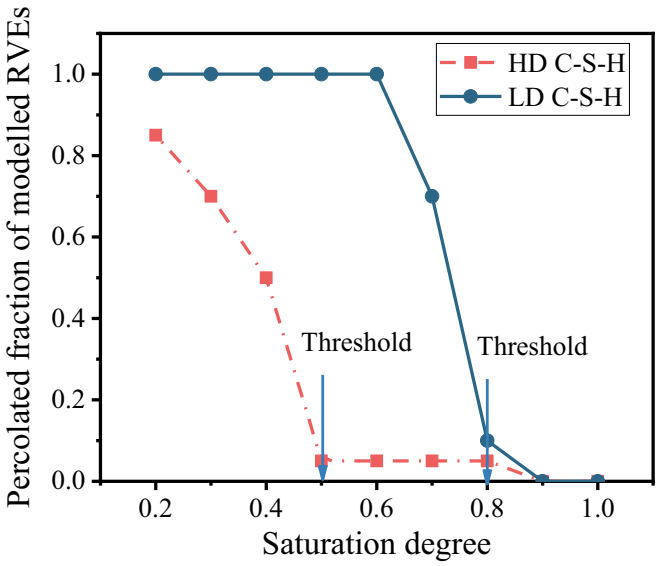

Fig. A.1. Percolated fraction of modelled RVEs: the ratio of the number of RVEs in which gas-filled pores can percolate the RVE to the total number of RVEs.

References

[1] Q.-f. Liu, Progress and research challenges in concrete durability: ionic transport, electrochemical rehabilitation and service life prediction, RILEM Tech. Lett. 7 (2022) 98–111.

[2] S. Bejaoui, B. Bary, Modeling of the link between microstructure and effective diffusivity of cement pastes using a simplified composite model, Cem. Concr. Res. 37 (3) (2007) 469–480.

[3] M. Ashraf, M.F. Iqbal, M. Rauf, et al., Developing a sustainable concrete incorporating bentonite clay and silica fume: mechanical and durability performance, J. Clean. Prod. 337 (2022), 130315.

[4] L. Tong, J. Zhao, Z. Cheng, Chloride ion binding effect and corrosion resistance of geopolymer materials prepared with seawater and coral sand, Construct. Build Mater. 309 (2021).

[5] Q.-F. Liu, G.-L. Feng, J. Xia, J. Yang, L.-Y. Li, Ionic transport features in concrete composites containing various shaped aggregates: a numerical study, Compos. Struct. 183 (2018) 371–380.

[6] X.-h. Shen, W.-q. Jiang, D. Hou, et al., Numerical study of carbonation and its effect on chloride binding in concrete, Cem. Concr. Compos. 104 (2019) 103402.

[7] L.-X. Mao, Z. Hu, J. Xia, et al., Multi-phase modelling of electrochemical rehabilitation for ASR and chloride affected concrete composites, Compos. Struct. 207 (2019) 176–189.

[8] Z. Meng, Q.F. Liu, J. Xia, Y. Cai, X. Zhu, Y. Zhou, L. Pel, Mechanical–transport–chemical modeling of electrochemical repair methods for corrosion-induced cracking in marine concrete, Comput. Aided Civ. Inf. Eng. 37 (14) (2022) 1854–1874.

[9] Y. Gan, H. Zhang, M. Liang, E. Schlangen, K. van Breugel, B. Šavija, A numerical study of fatigue of hardened cement paste at the microscale, Int. J. Fatigue 151 (2021).

[10] D. Dauti, S. Dal Pont, B. Weber, M. Briffaut, N. Toropovs, M. Wyrzykowski, G. Sciumé, Modeling concrete exposed to high temperature: impact of dehydration and retention curves on moisture migration, Int. J. Numer. Anal. Methods Geomech. 42 (13) (2018) 1516–1530.

[11] Q.F. Liu, Z. Hu, X.E. Wang, H. Zhao, K. Qian, L.J. Li, Z. Meng, Numerical study on cracking and its effect on chloride transport in concrete subjected to external load, Constr. Build. Mater. 325 (2022), 126797.

[12] M. Achour, F. Bignonnet, J.-F. Barthélémy, E. Rozière, O. Amiri, Multi-scale modeling of the chloride diffusivity and the elasticity of Portland cement paste, Construct. Build Mater. 234 (2020), 117124.

[13] C. Liu, F. Wang, M. Zhang, Modelling of 3D microstructure and effective diffusivity of fly ash blended cement paste, Cem. Concr. Compos. 110 (2020), 103586.

[14] Z.Z. Meng, Q.-F. Liu, N. Ukrainczyk, S. Mu, Y.F. Zhang, G.D. Schutter, Numerical study on the chemical and electrochemical coupling mechanisms for concrete under combined chloride-sulfate attack, Cem. Concr. Res. 175 (2024), 107368.

[15] L. Tong, Q. Liu, Modelling of concrete transport property by considering multi-scale heterogeneous characteristics, J. Build. Mater. 26 (10) (2023) 1062–1071.

[16] Q.X. Xiong, L.-y. Tong, F. Meftah, et al., Improved predictions of permeability properties in cement-based materials: a comparative study of pore size distribution-based models, Constr. Build. Mater. (2023), 133927.

[17] L.-y. Li, A pore size distribution-based chloride transport model in concrete, Mag. Concr. Res. 66 (18) (2014) 937–947.

[18] C.L. Page, N.R. Short, A. El Tarras, Diffusion of chloride ions in hardened cement pastes, Cem. Concr. Res. 11 (3) (1981) 395–406.

[19] Y. Zhang, M. Zhang, Transport properties in unsaturated cement-based materials – a review, Construct. Build Mater. 72 (2014) 367–379.

[20] L. Tang, L.O. Nilsson, A new approach to the determination of pore distribution by penetrating chlorides into concrete, Cem. Concr. Res. 25 (4) (1995) 695–701.

[21] L.-y. Tong, Q.-f. Liu, Q.X. Xiong, Z. Meng, O. Amiri, M. Zhang, Modelling the chloride transport in concrete from microstructure generation to chloride diffusivity prediction, Comput. Aided Civ. Inf. (2024).

[22] N. Neithalath, J. Jain, Relating rapid chloride transport parameters of concretes to microstructural features extracted from electrical impedance, Cem. Concr. Res. 40 (7) (2010) 1041–1051.

[23] H. Hornain, J. Marchand, V. Duhot, M. Moranville-Regourd, Diffusion of chloride ions in limestone filler blended cement pastes and mortars, Cem. Concr. Res. 25 (8) (1995) 1667–1678.

[24] A.V. Saetta, R.V. Scotta, R.V. Vitaliani, Analysis of chloride diffusion into partially saturated concrete, Mater. J. 90 (5) (1993) 441–451.

[25] E.P. Nielsen, M.R. Geiker, Chloride diffusion in partially saturated cementitious material, Cem. Concr. Res. 33 (1) (2003) 133–138.

[26] N. Olsson, V. Baroghel-Bouny, L.-O. Nilsson, M. Thiery, Non-saturated ion diffusion in concrete – a new approach to evaluate conductivity measurements, Cem. Concr. Compos. 40 (2013) 40–47.

[27] A. Buchwald, Determination of the ion diffusion coefficient in moisture and salt loaded masonry materials by impedance spectroscopy, in: 3rd Int. PhD Symposium, 2000.

[28] V. Baroghel-Bouny, M. Thiéry, X. Wang, Modelling of isothermal coupled moisture–ion transport in cementitious materials, Cem. Concr. Res. 41 (8) (2011) 828–841.

[29] N. Olsson, V. Baroghel-Bouny, L.-O. Nilsson, M. Thiery, Non-saturated ion diffusion in concrete–a new approach to evaluate conductivity measurements, Cem. Concr. Compos. 40 (2013) 40–47.

[30] B. Ghanbarian, A.G. Hunt, R.P. Ewing, M. Sahimi, Tortuosity in porous media: a critical review, Soil Sci. Soc. Am. J. 77 (5) (2013) 1461–1477.

[31] H. Chou, L. Wu, L. Zeng, A. Chang, Evaluation of solute diffusion tortuosity factor models for variously saturated soils, Water Resour. Res. 48 (10) (2012).

[32] Y. Zhang, G. Ye, Z. Yang, Pore size dependent connectivity and ionic transport in saturated cementitious materials, Construct. Build Mater. 238 (2020).

[33] Y. Guo, T. Zhang, J. Du, C. Wang, J. Wei, Q. Yu, Evaluating the chloride diffusion coefficient of cement mortars based on the tortuosity of pore structurally-designed cement pastes, Microporous Mesoporous Mater. 317 (2021).

[34] Z.Z. Meng, Y.F. Zhang, W.K. Chen, et al., A numerical study of moisture and ionic transport in unsaturated concrete by considering multi-ions coupling effect, Transp. Porous Media (2023), https://doi.org/10.1007/s11242-023-02011-6.

[35] R.A. Patel, J. Perko, D. Jacques, G. De Schutter, K. Van Breugel, G. Ye, A versatile pore-scale multicomponent reactive transport approach based on lattice Boltzmann method: application to portlandite dissolution, Phys. Chem. Earth A/B/C 70-71 (2014) 127–137.

[36] N. Ukrainczyk, E.A.B. Koenders, Representative elementary volumes for 3D modeling of mass transport in cementitious materials, Model. Simul. Mater. Sci. Eng. 22 (3) (2014), 035001.

[37] N.S. Martys, Diffusion in partially-saturated porous materials, Mater. Struct. 32 (8) (1999) 555–562.

[38] M. Zhang, G. Ye, K. van Breugel, Modeling of ionic diffusivity in non-saturated cement-based materials using lattice Boltzmann method, Cem. Concr. Res. 42 (11) (2012) 1524–1533.
[39] M. Zhang, G. Ye, K. van Breugel, Multiscale lattice Boltzmann-finite element modelling of chloride diffusivity in cementitious materials. Part I: algorithms and implementation, Mech. Res. Commun. 58 (2014) 53–63.
[40] M. Zhang, G. Ye, K. van Breugel, Multiscale lattice Boltzmann-finite element modelling of chloride diffusivity in cementitious materials. Part II: simulation results and validation, Mech. Res. Commun. 58 (2014) 64–72.
[41] R.A. Patel, Q.T. Phung, S.C. Seetharam, J. Perko, D. Jacques, N. Maes, G. De Schutter, G. Ye, K. Van Breugel, Diffusivity of saturated ordinary Portland cement-based materials: a critical review of experimental and analytical modelling approaches, Cem. Concr. Res. 90 (2016) 52–72.
[42] J. Perko, N. Ukrainczyk, B. Šavija, Q.T. Phung, E.A.B. Koenders, Influence of micro-pore connectivity and micro-fractures on calcium leaching of cement pastes—a coupled simulation approach, Materials 13 (12) (2020) 2697.
[43] G. Constantinides, F.-J. Ulm, The nanogranular nature of C–S–H, J. Mech. Phys. Solids 55 (1) (2007) 64–90.
[44] K. Scrivener, A. Ouzia, P. Juilland, A. Kunhi Mohamed, Advances in understanding cement hydration mechanisms, Cem. Concr. Res. 124 (2019), 105823.
[45] Q.F. Liu, M.F. Iqbal, J. Yang, X. Lu, P. Zhang, M. Rauf, Prediction of chloride diffusivity in concrete using artificial neural network: modelling and performance evaluation, Constr. Build. Mater. 268 (2021), 121082.
[46] L.-y. Tong, Q.X. Xiong, M. Zhang, Z. Meng, F. Meftah, Q.-F. Liu, Multi-scale modelling and statistical analysis of heterogeneous characteristics effect on chloride transport properties in concrete, Construct. Build Mater. 367 (2023), 130096.
[47] C. Liu, M. Zhang, Multiscale modelling of ionic diffusivity in unsaturated concrete accounting for its hierarchical microstructure, Cem. Concr. Res. 156 (2022), 106766.
[48] Q. Liu, Multi-phase modelling of concrete at meso-micro scale based on multi-species transport, J. Chin. Ceram. Soc. 46 (08) (2018) 1074–1080.
[49] Y. Cai, Q.-F. Liu, Stability of fresh concrete and its effect on late-age durability of reinforced concrete: an overview, J. Build. Eng. 179 (2023), 107701.
[50] Q.X. Xiong, F. Meftah, Determination on pore size distribution by a probabilistic porous network subjected to salt precipitation and dissolution, Comput. Mater. Sci. 195 (2021), 110491.
[51] D. Hou, Y. Jia, J. Yu, P. Wang, Q. Liu, Transport properties of sulfate and chloride ions confined between calcium silicate hydrate surfaces: a molecular dynamics study, J. Phys. Chem. C 122 (49) (2018) 28021–28032.
[52] P.J. McDonald, V. Rodin, A. Valori, Characterisation of intra- and inter-C–S–H gel pore water in white cement based on an analysis of NMR signal amplitudes as a function of water content, Cem. Concr. Res. 40 (12) (2010) 1656–1663.
[53] H.M. Jennings, A. Kumar, G. Sant, Quantitative discrimination of the nano-pore-structure of cement paste during drying: new insights from water sorption isotherms, Cem. Concr. Res. 76 (2015) 27–36.
[54] Y. Zhang, Z. Yang, G. Ye, Dependence of unsaturated chloride diffusion on the pore structure in cementitious materials, Cem. Concr. Res. 127 (2020).
[55] Y. Zhang, G. Ye, A model for predicting the relative chloride diffusion coefficient in unsaturated cementitious materials, Cem. Concr. Res. 115 (2019) 133–144.
[56] W. Dridi, Analysis of effective diffusivity of cement based materials by multi-scale modelling, Mater. Struct. 46 (1–2) (2012) 313–326.
[57] P.D. Tennis, H.M. Jennings, A model for two types of calcium silicate hydrate in the microstructure of Portland cement pastes, Cem. Concr. Res. 30 (6) (2000) 855–863.
[58] F.J. Ulm, G. Constantinides, F.H. Heukamp, Is concrete a poromechanics materials?—A multiscale investigation of poroelastic properties, Mater. Struct. 37 (1) (2004) 43–58.
[59] C. Liu, R. Qian, Z. Liu, G. Liu, Y. Zhang, Multi-scale modelling of thermal conductivity of phase change material/recycled cement paste incorporated cement-based composite material, Mater. Des. 191 (2020), 108646.
[60] G.W. Scherer, Structure and properties of gels, Cem. Concr. Res. 29 (8) (1999) 1149–1157.
[61] S. Babaei, S.C. Seetharam, U. Muehlich, A. Dizier, G. Steenackers, B. Craeye, A multiscale framework to estimate water sorption isotherms for OPC-based materials, Cem. Concr. Compos. 105 (2020), 103415.
[62] C. Liu, Z. Liu, Y. Zhang, A multi-scale framework for modelling effective gas diffusivity in dry cement paste: combined effects of surface, Knudsen and molecular diffusion, Cem. Concr. Res. 131 (2020), 106035.
[63] H.M. Jennings, Refinements to colloid model of C-S-H in cement: CM-II, Cem. Concr. Res. 38 (3) (2008) 275–289.
[64] Z. Jiang, Y. Xi, X. Gu, Q. Huang, W. Zhang, Modelling of water vapour sorption hysteresis of cement-based materials based on pore size distribution, Cem. Concr. Res. 115 (2019) 8–19.
[65] S. Bishnoi, K.L. Scrivener, μic: a new platform for modelling the hydration of cements, Cem. Concr. Res. 39 (4) (2009) 266–274.
[66] C. Liu, Z. Xu, G. Chen, L. Yang, Y. Zhang, J. Gao, Microscopic modelling of gas diffusivity in unsaturated cementitious materials considering multiple diffusion regimes, Int. J. Heat Mass Transf. 192 (2022), 122916.
[67] K.L. Scrivener, P. Juilland, P.J. Monteiro, Advances in understanding hydration of Portland cement, Cem. Concr. Res. 78 (2015) 38–56.
[68] L. Holzer, B. Muench, M. Wegmann, P. Gasser, R.J. Flatt, FIB-nanotomography of particulate systems—part I: particle shape and topology of interfaces, J. Am. Ceram. Soc. 89 (8) (2006) 2577–2585.
[69] H. Ma, D. Hou, Y. Lu, Z. Li, Two-scale modeling of the capillary network in hydrated cement paste, Construct. Build Mater. 64 (2014) 11–21.
[70] M. Zhang, G. Ye, K. Van Breugel, A numerical-statistical approach to determining the representative elementary volume (REV) of cement paste for measuring diffusivity, Mater. Constr. 60 (300) (2010) 7–20.
[71] D.P. Bentz, O.M. Jensen, A.M. Coats, F.P. Glasser, Influence of silica fume on diffusivity in cement-based materials: I. Experimental and computer modeling studies on cement pastes, Cem. Concr. Res. 30 (6) (2000) 953–962.
[72] D.P. Bentz, E.J. Garboczi, Percolation of phases in a three-dimensional cement paste microstructural model, Cem. Concr. Res. 21 (2) (1991) 325–344.
[73] L. Liu, H. Chen, W. Sun, G. Ye, Microstructure-based modeling of the diffusivity of cement paste with micro-cracks, Construct. Build Mater. 38 (2013) 1107–1116.
[74] Z. Zhang, M. Thiery, V. Baroghel-Bouny, Numerical modelling of moisture transfers with hysteresis within cementitious materials: verification and investigation of the effects of repeated wetting–drying boundary conditions, Cem. Concr. Res. 68 (2015) 10–23.
[75] L. Tong, Q. Liu, Prediction model for diffusivity of unsaturated concrete by considering time-varying pore structure, J. Chin. Ceram. Soc. 51 (8) (2023) 1950–1961.
[76] F. Xu, S. Liang, Y. Zhang, B. Li, Y. Hu, Numerical study of water–air distribution in unsaturated soil by using lattice Boltzmann method, Comput. Math. Appl. 81 (2021) 573–587.
[77] V. Pot, S. Peth, O. Monga, L.E. Vogel, A. Genty, P. Garnier, L. Vieublé-Gonod, M. Ogurreck, F. Beckmann, P.C. Baveye, Three-dimensional distribution of water and air in soil pores: comparison of two-phase two-relaxation-times lattice-Boltzmann and morphological model outputs with synchrotron X-ray computed tomography data, Adv. Water Resour. 84 (2015) 87–102.
[78] T. Gimmi, S.V. Churakov, Water retention and diffusion in unsaturated clays: connecting atomistic and pore scale simulations, Appl. Clay Sci. 175 (2019) 169–183.
[79] S. Yang, N. Ukrainczyk, A. Caggiano, E. Koenders, Numerical phase-field model validation for dissolution of minerals, Appl. Sci. (Switzerland) 11 (6) (2021).
[80] P. Agrawal, A. Mascini, T. Bultreys, H. Aslannejad, M. Wolthers, V. Cnudde, I. B. Butler, A. Raoof, The impact of pore-throat shape evolution during dissolution on carbonate rock permeability: pore network modeling and experiments, Adv. Water Resour. 155 (2021).
[81] M.J. Blunt, B. Bijeljic, H. Dong, O. Gharbi, S. Iglauer, P. Mostaghimi, A. Paluszny, C. Pentland, Pore-scale imaging and modelling, Adv. Water Resour. 51 (2013) 197–216.
[82] J. Weiss, K. Snyder, J. Bullard, D. Bentz, Using a saturation function to interpret the electrical properties of partially saturated concrete, J. Mater. Civ. Eng. 25 (8) (2013) 1097–1106.
[83] K. Li, M. Stroeven, P. Stroeven, L.J. Sluys, Investigation of liquid water and gas permeability of partially saturated cement paste by DEM approach, Cem. Concr. Res. 83 (2016) 104–113.
[84] Q. Huang, Z. Jiang, X. Gu, W. Zhang, B. Guo, Numerical simulation of moisture transport in concrete based on a pore size distribution model, Cem. Concr. Res. 67 (2015) 31–43.
[85] M. Wyrzykowski, P. Lura, F. Pesavento, D. Gawin, Modeling of water migration during internal curing with superabsorbent polymers, J. Mater. Civ. Eng. 24 (8) (2012) 1006–1016.
[86] L.H. Cohan, Sorption hysteresis and the vapor pressure of concave surfaces, J. Am. Chem. Soc. 60 (1938) 433–435.
[87] Q.X. Xiong, L.-Y. Tong, Z. Zhang, C. Shi, Q.-F. Liu, A new analytical method to predict permeability properties of cementitious mortars: the impacts of pore structure evolutions and relative humidity variations, Cem. Concr. Compos. 137 (2023), 104912.
[88] D. Li, W. Zhao, D. Hou, T. Zhao, Molecular dynamics study on the chemical bound, physical adsorbed and ultra-confined water molecules in the nano-pore of calcium silicate hydrate, Construct. Build Mater. 151 (2017) 563–574.
[89] P.T. Nguyen, O. Amiri, Study of the chloride transport in unsaturated concrete: highlighting of electrical double layer, temperature and hysteresis effects, Construct. Build Mater. 122 (2016) 284–293.
[90] B. Bary, S. Béjaoui, Assessment of diffusive and mechanical properties of hardened cement pastes using a multi-coated sphere assemblage model, Cem. Concr. Res. 36 (2) (2006) 245–258.
[91] A.T.C. Guimarães, M.A. Climent, G.D. Vera, F.J. Vicente, F.T. Rodrigues, C. Andrade, Determination of chloride diffusivity through partially saturated Portland cement concrete by a simplified procedure, Construct. Build Mater. 25 (2) (2011) 785–790.
[92] N. Olsson, B. Lothenbach, V. Baroghel-Bouny, L.-O. Nilsson, Unsaturated ion diffusion in cementitious materials – the effect of slag and silica fume, Cem. Concr. Res. 108 (2018) 31–37.
[93] F. Rajabipour, In Situ Electrical Sensing and Material Health Monitoring of Concrete Structures (PhD thesis), Purdue University, 2006.
[94] M. Shafikhani, S.E. Chidiac, A holistic model for cement paste and concrete chloride diffusion coefficient, Cem. Concr. Res. 133 (2020), 106049.
[95] A. Atkinson, A.K. Nickerson, The diffusion of ions through water-saturated cement, J. Mater. Sci. 19 (9) (1984) 3068–3078.